Eur. J. Mineral., 35, 1125–1147, 2023
https://doi.org/10.5194/ejm-35-1125-2023

European Journal of Mineralogy
Open Access

Retrogression of ultrahigh-pressure eclogite, Western Gneiss Region, Norway

Dirk Spengler[1], **Adam Włodek**[1], **Xin Zhong**[2], **Anselm Loges**[2], **and Simon J. Cuthbert**[1]

[1]Faculty of Geology, Geophysics and Environmental Protection, AGH University of Krakow, 30-059 Kraków, Poland
[2]Institut für Geologische Wissenschaften, Freie Universität Berlin, 12449 Berlin, Germany

Correspondence: Dirk Spengler (dirk@spengler.eu)

Received: 1 May 2023 – Revised: 11 September 2023 – Accepted: 20 October 2023 – Published: 14 December 2023

Abstract. The Western Gneiss Region (WGR) in western Norway exposes ultrahigh-pressure (UHP) eclogites that occur repeatedly, within an area of high-pressure (HP) eclogites, without evidence of being separated by tectonic shear or ductile flow structures. We studied 10 eclogites from two northern UHP areas and the interjacent HP area to evaluate the significance of this pattern. The orthopyroxene in orthopyroxene-bearing samples has low Al_2O_3 contents (0.17 wt %–0.37 wt %), provided its grain boundaries were unaffected by partial recrystallisation or replacement. Classical geothermobarometry based on element partitioning between coexisting mineral phases suggests metamorphic conditions within the diamond stability field for the samples from both the HP and UHP areas. The primary clinopyroxene in the associated orthopyroxene-free eclogites contains aligned inclusions of either needle-shaped quartz ± pargasite or lamellar albite, which are absent from the secondary (symplectic) clinopyroxene. Reconstructed mineral compositions of the primary clinopyroxene obtained from grain cross-section surfaces using a scanning electron beam or image processing are non-stoichiometric, and they have higher Ca-Eskola and lower Ca-Tschermak components than the inclusion-bearing host clinopyroxene. The molar ratios of these endmembers are consistent with the needles in the primary clinopyroxene being formed from vacancy-bearing precursor clinopyroxene by the exsolution reaction 2 Ca-Eskola = Ca-Tschermak + 3 quartz during early eclogite-facies retrogression. Further retrogression partially transformed the needle-shaped quartz to irregularly shaped albite within the clinopyroxene and partially transformed both clinopyroxene generations to amphibole that occasionally preserves the needles. The similarity of both the maximum metamorphic conditions and the mineral exsolution microstructures in the eclogites from UHP and HP areas indicates a shared metamorphic history within the stability field of diamond, but a history that diverged during retrogression. Consequently, the alternations of UHP and HP areas in the WGR may have formed by a process that allowed for spatial variations in retrogression efficiency, such as the localisation of strain (recrystallisation) or fluid flow (diffusion) or both, rather than by tectonic stacking of UHP and HP units. Evidence for the UHP metamorphism of WGR crustal rocks is now found from NE to SW along the entire coastal section that covers previously recognised UHP and interjacent areas.

1 Introduction

An understanding of the tectonic evolution of an orogen relies strongly on the pressure and temperature information obtained from metamorphic rocks. An impressive example of such information is the first discovery of coesite, a polymorph of quartz stable at pressures greater than ∼ 2.5 GPa, within blueschists and eclogites in subducted continental crust (Chopin, 1984; Smith, 1984). These reports confirmed earlier propositions about the potential intensity of crustal metamorphism (Lappin and Smith, 1978, 1981) and ultimately led to a dramatic rescaling of our perceptions about the depth to which parts of the Earth's crust were temporarily subducted during the Alpine and Caledonian orogenies prior to exhumation. Subsequent reports of similar ultrahigh-

pressure (UHP) metamorphic areas defined by the occurrence of coesite showed that this is a common feature in many orogens worldwide, but mainly of Phanerozoic age (Brown, 2007). The size and extent of these UHP metamorphic areas seem to matter, as any differences may relate to their formation at different stages of the orogeny and be influenced by tectonic parameters, such as convergence rates and angles (Kylander-Clark et al., 2012). However, the physical mechanisms of the exhumation of UHP rocks are less well understood. This is partially related to the paucity of UHP indicators (such as index minerals or corresponding geothermobarometric estimates) in most of the rock volume associated with UHP rocks. Therefore, the metamorphic record in these areas often appears to be bimodal in terms of metamorphic pressure, which leads to the question of whether high-pressure (HP) rocks were ever subjected to UHP metamorphic conditions.

There are mainly two possible explanations for this bimodality: (i) the exhumation of UHP rocks as isolated rock bodies (lenses) in a tectonic mélange (Lappin and Smith, 1978, 1981; Dobretsov et al., 1995) within a subduction/exhumation channel (Warren et al., 2008; Duretz et al., 2012) and (ii) their exhumation as large coherent units that were perhaps tectonically thrust onto each other (Wain et al., 2000; Hacker et al., 2010; Young, 2018). Evidence for the first explanation has been based mainly on thermo-mechanical numerical experiments (Gerya et al., 2008). The second explanation has been supported by the broader picture provided by geological data that include metamorphic gradients and structures (Krogh, 1977; Griffin et al., 1985). However, a combination of both endmember models (i.e. coherent UHP units surrounded by ductile HP units in between plate interfaces) may also apply, as suggested by numerical modelling (Yamato et al., 2008). Alternatively, the major differences in metamorphic records between closely associated rocks could simply relate to spatial variations in the degree of preservation of maximum metamorphic conditions, which would make the contrast between areas of HP and UHP metamorphism a secondary feature. It follows that detailed knowledge of both the peak metamorphism and the retrogression of high-grade rocks is essential if we are to recognise (i) the extent of areas that include rocks that once experienced UHP metamorphic conditions and (ii) the significance of the apparent metamorphic bimodality, which ultimately led to a pattern of alternating UHP and HP areas in the Western Gneiss Region (WGR) of Norway (Fig. 1), for tectonic exhumation models. For this study, we focused on the mineral chemistry and microstructures of 10 eclogites occurring within and between the two northern UHP areas in the WGR to assess the evolutionary similarities and differences of the samples in relation to their spatial occurrence.

2 Geological setting and sample localities

The Caledonides in Scandinavia were formed in response to the early Palaeozoic closure of the Iapetus Ocean and the subsequent collision of the continents of Laurentia and Baltica (Gee et al., 2013). This collision caused the thrusting of nappes with peripheral, outboard, and Laurentian affinities onto the Baltica plate margin, where they formed an east-verging tectono-stratigraphic succession (Gee et al., 1985). The WGR constitutes a tectonic window through this nappe pile onto the lowermost tectono-stratigraphic unit (the Lower Allochthon), and it exposes high-grade metamorphic rocks with Proterozoic protolith ages (Kullerud et al., 1986; Tucker et al., 1990). These Proterozoic Baltica basement gneisses, together with minor infolded supracrustal rocks (Krill, 1980), were reworked during the Caledonian orogeny. Radiogenic ages from high-grade quartzo-feldspathic gneisses and enclosed lenses of deformed mafic and ultramafic rocks (eclogite and pyroxenite) suggest that the culmination of plate convergence occurred during the final stage of orogenesis, the Scandian phase, during the Silurian and early Devonian under UHP metamorphic conditions (Griffin and Brueckner, 1980; Carswell et al., 2003b; Tucker et al., 2004; Spengler et al., 2009).

The nature of the spatiotemporal variations of this UHP metamorphism in the WGR, including the intensity, is less well known. For instance, radiometric ages form clusters at single outcrops (Walczak et al., 2019), age populations appear to shift between different outcrops (March et al., 2022), and age ranges obtained from the high-grade metamorphic rocks are often relatively broad (Kylander-Clark et al., 2007). These observations suggest either a prolonged period of subduction and exhumation or multiple events of temporary subduction and exhumation that perhaps affected individual units differently during the Caledonian orogeny, thus adding complexity to the tectonic geometry. Another complication relates to the completeness of the metamorphic record, which appears to be biased by the whole-rock chemistry. WGR felsic rocks (gneisses) generally preserve little or no evidence of the UHP metamorphism, with a few exceptions (Dobrzhinetskaya et al., 1995; Wain et al., 2000; Schönig et al., 2018) in felsic rocks solely from the coastal area of the WGR where the index minerals diamond and coesite occur (as well as the polycrystalline quartz that results from the coesite-to-quartz transformation). Most bimineralic and other orthopyroxene-free eclogites preserve evidence for UHP metamorphism in the form of index minerals and geothermobarometric estimates that hardly exceed the graphite–diamond phase transition (Smith, 1984; Smith and Lappin, 1989; Wain, 1997; Carswell et al., 2003b; Young et al., 2007). The more mafic (orthopyroxene-bearing) eclogites have been shown phenomenologically to preserve systematically higher peak metamorphic conditions than do the bimineralic eclogites (Lappin and Smith, 1978; Cuthbert et al., 2000), although the reason for this is unknown. In-

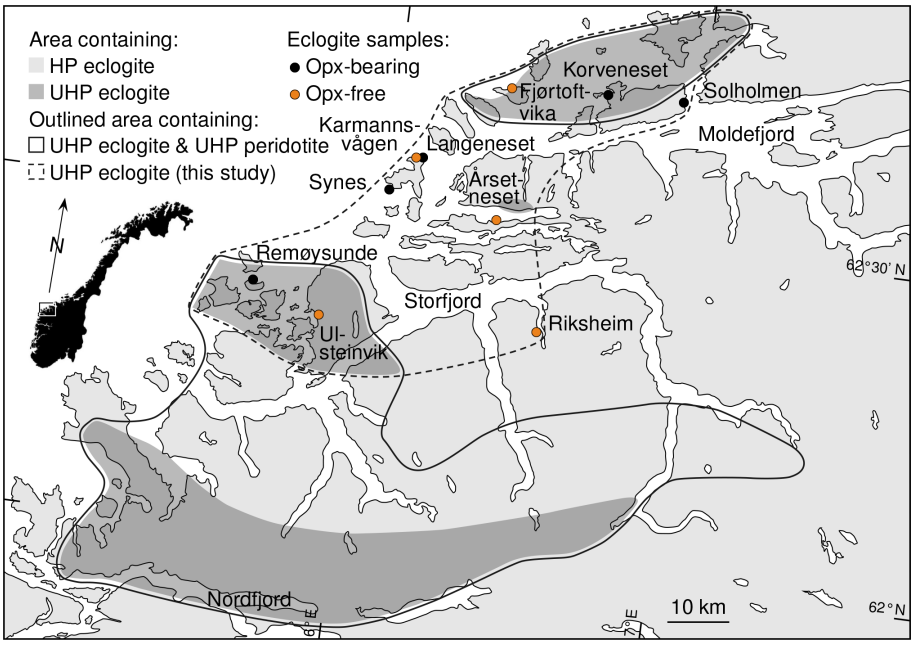

Figure 1. Simplified map of W Norway that shows sample locations and the distribution of areas that contain UHP eclogite (Smith, 1988; Spencer et al., 2013) and those that contain both UHP eclogite and UHP peridotite (Spengler et al., 2021).

dex minerals are virtually absent mainly due to the lack of free silica in the mineral assemblages, but for many samples the mineral chemistry and the application of geothermobarometry have yielded estimates that clearly exceed the graphite–diamond phase transition. The highest UHP metamorphic conditions, deep in the stability field of diamond, seem to be preserved in the mineral chemistry of ultramafic rocks (Cuthbert et al., 2000; Spengler et al., 2009), and the reasons for this may include the general rheological strength of orthopyroxene during deformation (Terry and Heidelbach, 2006) and issues related to large orthopyroxene grain sizes in combination with the sluggish diffusion of elements such as Al and Ca (Chin et al., 2015; Cherniak and Liang, 2022) that provide sensitive records of metamorphic conditions (Brey and Köhler, 1990).

These lithologically biased discrepancies in recorded (or preserved) metamorphic conditions have led to the following evolutionary scenarios. (i) If more importance is attached to the gneiss data, then the UHP metamorphism seems to have affected this rock type only at a few exotic spots along the coast, while the tectonic evolution of most of the gneiss was widely decoupled from that of the mafic to ultramafic rocks enclosed within the gneiss (Liu and Massonne, 2019). (ii) Alternatively, if more importance is attached to the eclogite data, then the spatial distribution of the eclogites suggests the presence of three discrete UHP metamorphic areas along the WGR coast that extend into the hinterland (Root et al., 2005). Whether felsic rocks and their enclosed mafic rocks had a cogenetic tectonic evolution depends solely on the exhumation mechanism. (iii) If the correlation between recorded metamorphic pressures and the effectiveness of chemical diffusion in the minerals of ultramafic rocks is considered, then two of the three UHP areas merge into one large area that extends even farther into the hinterland (Fig. 1; Spengler et al., 2021). By implication, many HP eclogites probably have an unrecognised UHP history that was erased by diffusion during exhumation, irrespective of the exhumation mechanism.

In the present study, sample locations were chosen so that gaps in the distribution of UHP metamorphic rocks became filled and a direct comparison of samples from HP and UHP areas could be achieved (Fig. 1). The coordinates of sample locations are given in Table 1. Details in the form of scanned thin sections of samples are presented in the Supplement, File S1. Five samples (M65, DS0326, 2-4A, DS1438, and UL-96-2) are from outcrops that have previously been studied. The other samples are from outcrops not previously described. The usage of the term "eclogite" is in accordance with common practice, i.e. mineral assemblage and mineral chemistry that may include clinopyroxene with < 20 mol % Na-pyroxene component (cf. Fig. 8 in Coleman et al., 1965).

Korveneset (Otrøy). Sample M65 is from a slightly retrogressed coarse-grained eclogite pod about 2.0 m × 1.5 m in dimensions, which occurs within mylonitic orthogneiss in a roadside quarry on the island of Otrøy close to Magerøysundet. This eclogite lens was previously studied by Carswell et al. (1985) and Carswell et al. (2006, sample Dap3.9).

Langeneset (Vigra). Sample DS2216 is from a mafic body a few tens of metres in size on the northern coast of the island of Vigra. The orthopyroxene-bearing eclogite shows strong retrogression that is visible to the naked eye. The rock has

been partially transformed to garnet amphibolite, and it is surrounded by a strongly banded gneiss of leucocratic and mafic compositions.

Remøysunde (Remøy). Sample DS0326 is from an outcrop of eclogite on the northern coast of the island of Remøy about 50 m to the east of the bridge to Runde. This eclogite lens is several metres in diameter, heterogeneous in composition, has individual crystals up to a few centimetres in size, and its margin has been amphibolitised. The locality was described in more detail by Robinson et al. (2003, Stop 1-4) and Quas-Cohen (2014, garnet websterite sample QC29).

Solholmen (Otrøy). Sample 2-4A is part of an eclogite that was exposed near the ferry harbour Solholmen on the island of Otrøy, but it is no longer accessible because it is covered by the extension to the ferry terminal car park. The locality was previously described by Carswell et al. (1985, samples U206 and U243).

Synes (Vigra). Sample DS1409 is part of an eclogite lens, ca. 10 m in diameter, which is exposed on the shoreline southwest of the Vigra Fjordhotell. It is safely accessible at low tide. The core of the lens is homogeneous in texture and consists of crystals of up to a few centimetres in size, whereas the periphery of the lens appears to have been recrystallised to smaller grain sizes. The degree of amphibolitisation increases towards the rim of the lens.

Fjørtoftvika (Fjørtoft). Sample DS1438 is part of an eclogite lens 5 m × 8 m in size that is located on the northern coast of the island of Fjørtoft at the northeastern edge of Fjørtoftvika. The lens grades from an eclogite-facies core to an amphibolite-facies rim, and it has been described in detail by Terry et al. (2000, kyanite–zoisite eclogite sample 1066b). The sample for our study was a loose piece of fresh coarse-grained eclogite obtained from this lens.

Karmannsvågen (Vigra). Sample DS2217 is a part of a 3 m × 5 m mafic lens that crops out on the northern shoreline of Vigra west of the bay of Karmannsvågen. Retrogressed eclogite makes up the core of the lens and the margin is amphibolitised. The lens is surrounded by banded gneiss.

Riksheim. Sample DS1405 is from a mafic lens about 6 m in diameter that was exposed in 2014 in a quarry of banded gneiss about 700 m west of Riksheim, on the mainland. The quarry is located at the end of the road that follows the Riksemelva upstream to Skasvødelva, and it is situated along its northern bank. The sample is a fine-grained partially amphibolitised eclogite.

Ulsteinvik (Hareidland). Sample UL-96-2 is part of a previously studied large eclogite body that crops out over an area of 6 km × 1.5 km on Hareidland and Dimnøy islands (Grønlie et al., 1972; Mysen and Heier, 1972; Carswell et al., 2003b).

Årsetneset (Ellingsøy). Sample DS2204 is from a ca. 150 m × 200 m mafic body that forms the tip of a rocky headland on the northern coast of Ellingsøy. Garnet amphibolite dominates the outcrop. The cliff on the northwestern side of the headland exposes a foliated retrogressed eclogite

Table 1. Sample locations (datum WGS84, UTM zone 32V) and minerals determined in thin sections by optical and electron microscopy and Raman spectroscopy, subdivided by paragenesis and microstructure: primary – eclogite-facies minerals, oriented inclusions – hosted by eclogite-facies minerals, secondary – retrograde (post-eclogite-facies) minerals. Amp – amphibole, Apt – apatite, Bt – biotite, Cpx – clinopyroxene, Grt – garnet, Ky – kyanite, Opaque – ilmenite in sample DS2217 and unspecified opaque minerals in all others, Opx – orthopyroxene, Pl – plagioclase, Qtz – quartz, Rt – rutile.

Sample no.	Locality (island)	Area	Easting (m)	Northing (m)	Precision (± m)	Grt	Opx	Cpx	Ky	Apt	Qtz	Rt	Opaque	Amp	Pl	Bt
Opx-bearing eclogite																
M65	Korveneset (Otrøy)	UHP	381 243	6 956 390	∼ 5	+	+	+			L	–	L s			s
DS2216	Langeneset (Vigra)	HP	351 848	6 943 241	5	+	+ (L)	+			(L)		–	(L) s	s	s
DS0326	Remøysunde (Remøy)	UHP	325 745	6 920 821	∼ 10	+	+	+			L	–	–	L s	s	
2-4A	Solholmen (Otrøy)	HP				+	+	+				–	–	L s		
DS1409	Synes (Vigra)	HP	346 880	6 937 338	2	+	+ L	+			L	–	–	L s	s	s
Opx-free eclogite																
DS1438	Fjørtoftvika (Fjørtoft)	UHP	365 914	6 956 067	5	+		+	–		+ L	–		L s		
DS2217	Karmannsvågen (Vigra)	UHP	351 514	6 943 304	3	+		+		–	–	–	+	s	L s	
DS1405	Riksheim (mainland)	HP	373 545	6 915 969	10	+		+ s			– L	–	–	s	s	s
UL-96-2	Ulsteinvik (Hareidland)	UHP				+		+ s	–		– L	–	–	s	s	
DS2204	Årsetneset (Ellingsøy)	HP	365 502	6 934 082	6	+		+			+ L	–	–	s	s	s

+ major primary phase, – accessory primary phase, L-oriented inclusions in Cpx, s – secondary phase, (L) inclusion unproven by electron microscopy/Raman spectroscopy.

Table 2. Calculated pyroxene endmembers.

Name	Abbreviation	Formula
Ca-Eskola	CaEs	$Ca_{0.5}\square_{0.5}AlSi_2O_6$
Ca-Tschermak	CaTs	$CaAl_2SiO_6$
Ti-pyroxene*	Ti-Cpx	$Na(Mg,Fe^{2+})_{0.5}Ti^{4+}_{0.5}Si_2O_6$
K-pyroxene	K-Cpx	$KAlSi_2O_6$
kosmochlor	Kos	$NaCrSi_2O_6$
jadeite	Jd	$NaAlSi_2O_6$
aegirine	Ae	$NaFe^{3+}Si_2O_6$
johannsenite	Jhn	$CaMn^{2+}Si_2O_6$
enstatite	En	$Mg_2Si_2O_6$
ferrosilite	Fs	$Fe_2Si_2O_6$
wollastonite	Wo	$Ca_2Si_2O_6$

* Katayama et al. (2000).

that is transected by quartz veins. Millimetre- to centimetre-thick foliation-parallel layers, rich in biotite, record zones of increased retrogression. The mafic body is surrounded by a migmatitic gneiss that has occasional mafic layers of garnet amphibolite.

3 Methods

The major and minor element contents of the minerals in our samples were determined using a JEOL JXA-8230 electron microprobe equipped with five spectrometers for wavelength dispersive spectrometry (WDS) at the Faculty of Geology, Geophysics and Environmental Protection, AGH University of Kraków, Kraków, Poland. Operating conditions were a 15 kV accelerating voltage and a beam current of 15 nA for feldspar and amphibole, 20 nA for garnet and pyroxene, and 100 nA for chemical mapping of mineral surface areas. The electron beam was generally either focused or defocused to 1 µm, but to 5 µm in the case of matrix feldspar. For point analyses, counting times per element in WDS mode were 20 s in the peak position and 10 s on either side of the peak, except for Na, for which the times were 10 and 5 s, respectively. Na was always the first element to be measured. Mineral surface areas with exposed inclusions were analysed using an integrative approach in WDS mode with a moving beam that scanned individual tiles ("points") ranging in size from $9 \times 9\,\mu m^2$ to $20 \times 20\,\mu m^2$. Several adjacent tiles formed a grid, and grid sizes ranged from 4×9 to 10×13 tiles. Grid compositions were obtained from the average of the compositions of the tiles in a grid. For chemical mapping, the dwell time per pixel of 0.5–4.0 µm edge length was 50–100 ms. External calibrations were made against international oxide and silicate standards.

Pyroxene compositions in wt % were transformed to mole proportions of 11 endmembers using all analysed cations (Table 2). The calculations were based on the numbers of cations per six oxygen anions. At first, all Fe was regarded as ferrous (Fe^{2+}), which minimises the cation deficiency from the ideal stoichiometric cation sum of four for CaEs-bearing pyroxene (Page et al., 2005). Subsequently, the CaEs component was assumed to reflect twice the deficiency of the cation sum from ideal stoichiometry: $CaEs = 2 \times (4 - \sum cations)$, provided there is sufficient Al (CaEs < Al). This served as a minimum estimate for the CaEs component. All Ti was assumed to be tetravalent with $Ti\text{-}Cpx = 2 \times Ti$, given that there is sufficient Na (Ti-Cpx < Na). Then all K was assumed to form K-Cpx, provided there is sufficient remaining Al ($K\text{-}Cpx = K < Al - CaEs$). Similarly, all Cr was assumed to form Kos, provided there is sufficient remaining Na ($Kos = Cr < Na - Ti\text{-}Cpx$). The Jd component was then assigned as the lower of the two values of either remaining Na ($= Na - Ti\text{-}Cpx - Kos$) or remaining Al ($= Al - CaEs - K\text{-}Cpx$). If all remaining Na was used up for Jd, then the excess Al forms $CaTs = 0.5 \times (Al - CaEs - K\text{-}Cpx - Jd)$. Alternatively, if all remaining Al was used up for Jd, then the excess Na forms $Ae = Na - Ti\text{-}Cpx - Kos - Jd$. In the former case, any conversion of Fe^{2+} to Fe^{3+} would result in a lack of available Na and require either an additional endmember or a smaller Jd component. However, in the latter case, the presence of calculated Ae requires ferric Fe. Only for these Ae-bearing pyroxenes, the ratio Fe_2O_3/FeO_{total} was increased from zero to a value such that the proportion of Fe^{3+} per six O became just equal to that of Ae. Both cases serve as minimum estimates for Ae as any additional Fe^{3+} would further lower the total cation sum and form Ae at the expense of Jd, which frees Al to become accommodated in CaEs. Thus, the proportions of Ae and CaEs correlate positively and form minimum estimates in this calculation scheme. Mn was regarded as divalent and forms Jhn ($Jhn = Mn$). Assuming Mg and Fe^{2+} have equal proportions within Ti-Cpx, En becomes half of the remaining Mg ($En = 0.5 \times (Mg - Ti\text{-}Cpx/4)$) and Fs becomes half of the remaining Fe^{2+} ($Fs = 0.5 \times (Fe^{2+} - Ti\text{-}Cpx/4)$). The Wo component is then half of the remaining Ca ($Wo = 0.5 \times (Ca - Jhn - CaTs - CaEs/2)$).

Raman spectra were obtained with an alpha300 R confocal Raman imaging system (WITec) in combination with a 532 nm Nd-YAG laser (Lambda Physik) at the Freie Universität Berlin. Gratings of 600 and 1800 grooves mm^{-1} (BLZ = 500 nm) were used to cover spectral ranges of 3800–100 and 1200–100 cm^{-1}, respectively. The instrument was calibrated using an internal Hg–Ar lamp before each experimental session. Raman spectra of the minerals were compared with those available from the open-access RRUFF database (Lafuente et al., 2015) and published data.

4 Results

4.1 Petrography

4.1.1 Orthopyroxene-bearing eclogite

Five samples (Korveneset, Langeneset, Remøysunde, Solholmen, and Synes) contain primarily garnet, clinopyroxene, and orthopyroxene as major components and rutile and opaque minerals as accessory minerals (Table 1). Quartz is absent as a primary mineral phase. The primary minerals are coarse grained. Grain sizes typically range from several 100 µm to a few millimetres and, in exceptional cases, ∼ 2 cm. These minerals have annealed grain boundaries and form granoblastic to foliated textures. Parts of the coarsest grains are inclusion-rich and poikiloblastic, indicative of an inherited older texture (Fig. 2a–d). All three major minerals have inclusions of each other so that garnet occurs as inclusions in clinopyroxene and orthopyroxene, and vice versa. The largest grains have inclusions with skeletal or irregular grain shapes, and in some cases, large clinopyroxene grains have parallel lamellae of orthopyroxene up to 40 µm thick. In contrast, elongated grains are mainly free of primary mineral inclusions, but the few inclusions that exist are typically elongated parallel to the long axis of the host (Fig. 2e, f).

In addition, the cores of both poikiloblastic and granoblastic/elongated clinopyroxene grains contain bimineralic inclusions that are acicular, with the needles a few micrometres thick and oriented parallel to each other (Fig. 3c–f). Raman micro-spectroscopy identified these oriented acicular inclusions as quartz and pargasite (Fig. 3g), and cross-section surfaces show them to be closely intergrown (Fig. 3d, f).

The extent of retrogression varies among the samples. Amphibole occurs as a secondary mineral and partially replaced clinopyroxene at its periphery. Another secondary mineral is biotite, which occurs mainly along grain boundaries, and which together with the amphibole is concentrated along discrete foliation-parallel layers. Partial replacements of rutile by ilmenite at grain margins were not observed. Plagioclase partially replaced primary minerals, and in the Langeneset sample it forms a fine-grained matrix that hosts coarse relic grains of garnet, clinopyroxene, and orthopyroxene. The proportion of secondary minerals in the Langeneset sample is higher than in the other samples (cf. Fig. 8a–c).

4.1.2 Orthopyroxene-free eclogite

The five samples from Fjørtoftvika, Karmannsvågen, Riksheim, Ulsteinvik, and Årsetneset have primary mineral assemblages dominated by garnet and clinopyroxene with accessory rutile, apatite, kyanite, and opaque minerals (Table 1). Individual samples may contain quartz or ilmenite as additional major constituents, thereby mirroring the whole-rock chemical variability of the orthopyroxene-free eclogites. These primary minerals, including ilmenite, have grain sizes of ∼ 200 µm to several millimetres (Fig. 4). Garnet, clinopyroxene, and kyanite may all contain each other as inclusions. Some samples from UHP areas have inclusions of irregularly shaped garnet, skeletal clinopyroxene (Fig. 4a), and kyanite (not shown), while large (> 100 µm) quartz inclusions are polycrystalline and solitary in occurrence (Fig. 4c). In contrast, samples from the HP area do not contain skeletal or polycrystalline inclusions, but small (< 50 µm) inclusions of quartz do occur, sometimes in high density (Fig. 4d). The major minerals form granoblastic textures with a weak foliation in eclogites from UHP areas, but with a clearly developed foliation in the eclogites from the HP area (Fig. 4; File S1).

The core of primary clinopyroxene contains oriented inclusions that are either monomineralic (Fig. 5) or bimineralic (Fig. 3a, b). The bimineralic inclusions are petrographically and mineralogically indistinguishable from those in the orthopyroxene-bearing eclogites (Fig. 3c–f), but the former, monomineralic inclusions vary in morphology between short-prismatic and acicular to lamellar shapes. Raman spectra identified these mineral inclusions as quartz, albite, and α-cristobalite (Fig. 5g). The inclusion–host interface relationships can be used to subdivide the inclusions. Inclusions with straight grain boundaries are either quartz or albite, while inclusions with irregular interfaces are albite or cristobalite (Fig. 5; File S2). Microstructural relationships (Fig. 5a) and Raman spectra, which show a mix of albite and quartz (spectrum 7 in Fig. 5g), suggest that the oriented mineral inclusions with straight grain boundaries were partially replaced by minerals with irregular grain boundaries against the host.

Grains of primary clinopyroxene were partially replaced by amphibole (Fig. 4b–d) and symplectites of secondary clinopyroxene and plagioclase (Fig. 4a, e, f). Depending on sample occurrence, these symplectites either have thin lamellae (Fig. 4a, e) or granular textures (Fig. 4f). The rims of garnet grains in some samples are surrounded or replaced by plagioclase and amphibole (Fig. 4b). Partial replacements of rutile by ilmenite at grain margins were not observed.

4.2 Chemistry of the primary minerals

4.2.1 Garnet

The garnet in our samples is compositionally zoned. Major element oxide contents show weak gradients in grain cores and commonly stronger gradients in the rims (Fig. 6c). The rims typically have oxide contents that are higher in FeO and lower in MgO and CaO. The average compositions of the grain cores of garnet in the orthopyroxene-bearing eclogites are $Prp_{42–58}Alm_{31–47}Grs_{9–16}Sps_{1}$, and in the orthopyroxene-free eclogites they are $Prp_{18–50}Alm_{17–59}Grs_{21–32}Sps_{0–2}$ (subscript numbers refer to mol %; the abbreviations refer to the garnet endmembers pyrope, almandine, grossular, and spessartine). These endmember proportions outline low-Ca and high-Ca compositional trends, respectively, and each compositional group of garnet covers two compositional

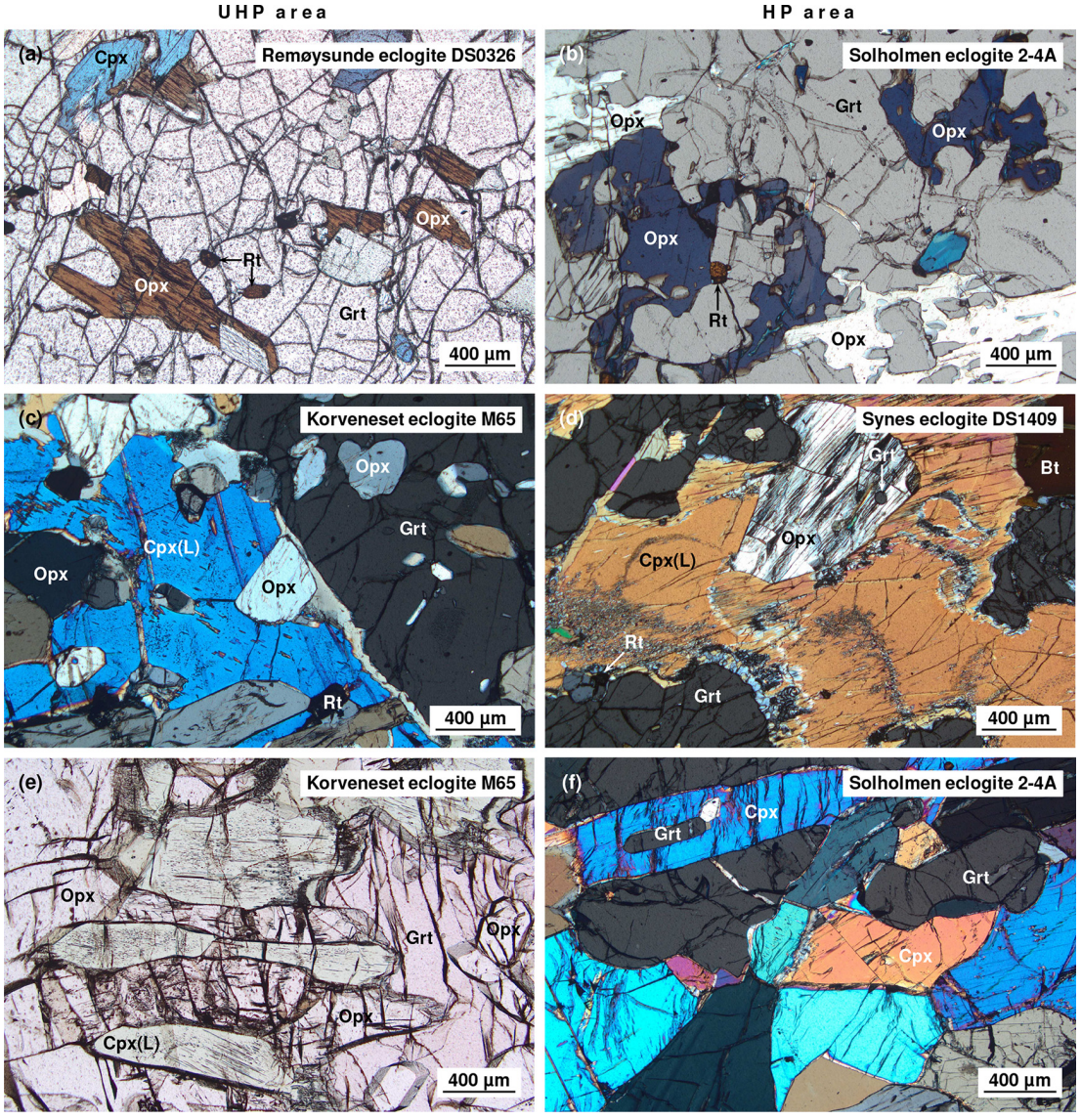

Figure 2. Primary mineral textures in WGR orthopyroxene-bearing eclogites from UHP **(a, c, e)** and HP **(b, d, f)** areas (sample details are given in each panel). **(a, b)** Skeletal orthopyroxene inclusions in garnet (obliquely cross-polarised light, same colour – same angle of extinction). **(c, d)** Poikiloblastic clinopyroxene (nearly cross-polarised light). **(e, f)** Elongated grain shapes define a foliation (**e** – in plane-polarised light, **f** – in nearly cross-polarised light). Cpx(L), clinopyroxene with oriented lamellae. Other mineral abbreviations are as in Table 1.

groups of eclogite (Fig. 6a), using the classification of Coleman et al. (1965). The Cr_2O_3 contents of the garnet grains have larger ranges in the orthopyroxene-bearing than in the orthopyroxene-free eclogites, specifically from the detection limit to 0.86 wt % and 0.07 wt %, respectively (Table 3). Each of these two compositional ranges forms a separate chemical trend on diagrams of garnet CaO versus Cr_2O_3 contents (Fig. 6b).

4.2.2 Clinopyroxene

Grains of clinopyroxene with oriented inclusions are compositionally zoned. The cores have relatively homogeneous major element contents (Fig. 7c), but the grain rims show variations in the form of Na_2O and Al_2O_3 contents that drop sharply while CaO contents increase sharply. The largest crystals with grain sizes of > 1 mm may have compositions that double in Al_2O_3 content from cores to inner rims, while Na_2O contents increase minimally (Fig. 7c). The contents of CaO are inversely proportional to those of Al_2O_3. Grain cores contain on average calculated endmember proportions

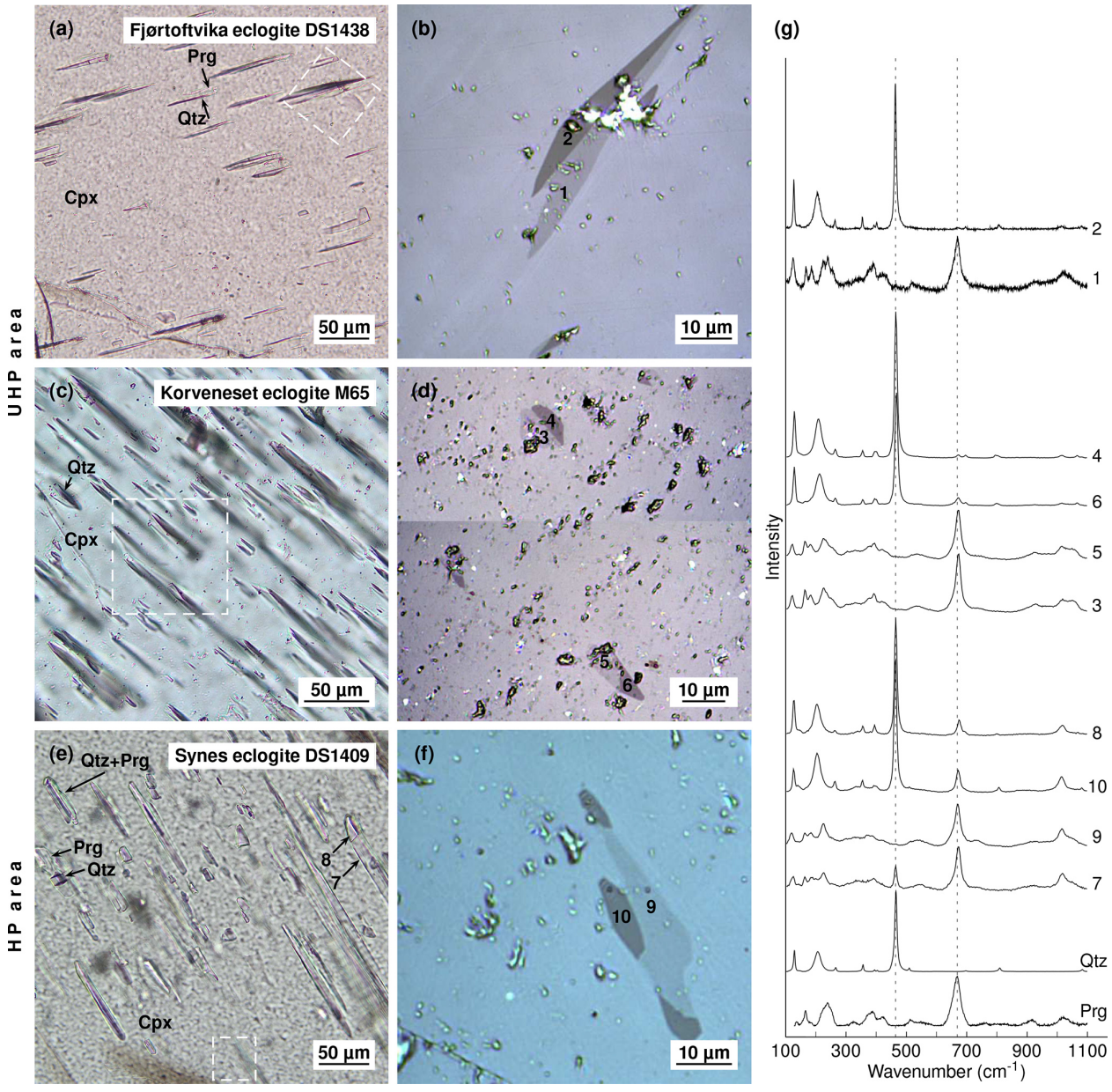

Figure 3. Oriented bimineralic inclusions in clinopyroxenes of WGR eclogites in plane-polarised light **(a, c, e)**, reflected light **(b, d, f)**, and related Raman spectra **(g)**. **(a, b)** Orthopyroxene-free eclogite. **(c–f)** Orthopyroxene-bearing eclogite. Dashed squares outline magnified regions shown in adjacent panels. **(g)** Raman spectra obtained at positions labelled in **(a)–(f)**. Dashed lines show the main peak positions in the reference spectra for Qtz (464 cm^{-1}) and pargasite (Prg; 669 cm^{-1}) obtained from the RRUFF database (Lafuente et al., 2015). Speckles in **(b)**, **(d)**, and **(f)** are reflections due to uneven surface polishing. Mineral abbreviations are as in Table 1.

of $Jd_{5–26}Ae_{0–13}En_{30–43}Fs_{4–8}Wo_{30–42}$ for orthopyroxene-bearing eclogites and $Jd_{0–46}Ae_{0–6}En_{22–39}Fs_{2–15}Wo_{23–41}$ for orthopyroxene-free eclogites (Table 4; Fig. 7a). Lamellae-bearing clinopyroxene grains in these two eclogite subsets have Ca-Tschermak components in the ranges of 0.1 mol %–4.0 mol % and 1.2 mol %–6.6 mol %, respectively, and low Ca-Eskola components of 0.0 mol %–3.1 mol % (Table 4). Reconstructed mineral core compositions (host + oriented inclusions) have lower Ca-Tschermak components than the host and higher Ca-Eskola components of 1.1 mol %–13.5 mol % (Table 5; Fig. 7b).

4.2.3 Orthopyroxene

The orthopyroxene grains are magnesian ($En_{73–86}$; Table 6), and they show intragranular compositional variations that depend on grain size and the proportion of secondary minerals in the sample. The largest grains (millimetre-size) in

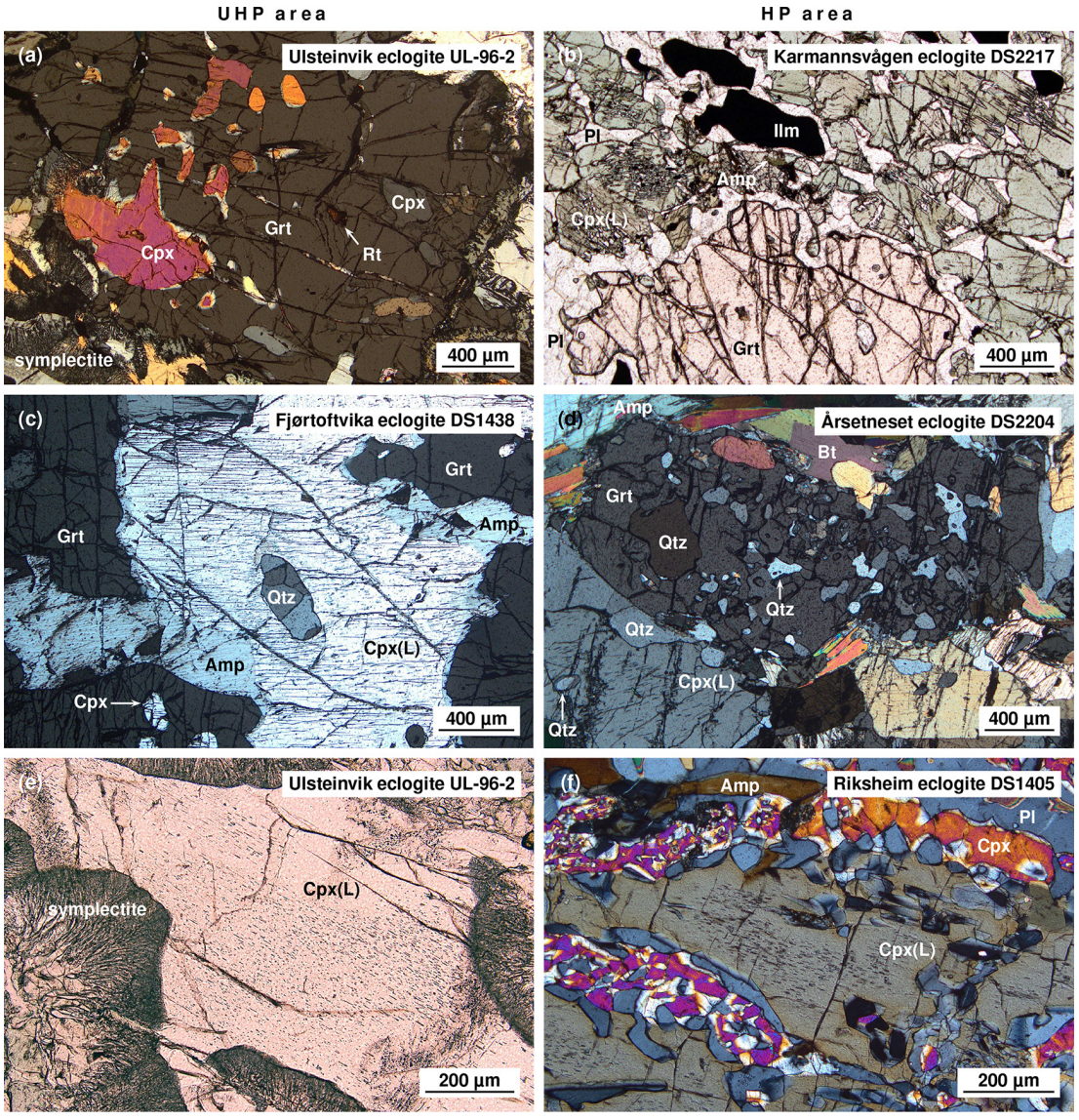

Figure 4. Primary mineral textures in WGR orthopyroxene-free eclogites from UHP **(a, c, e)** and HP **(b, d, f)** areas (sample details are given in each panel). **(a)** Skeletal clinopyroxene in coarse garnet (nearly cross-polarised light). **(b)** Short-prismatic clinopyroxene with oriented inclusions that define a foliation (plane-polarised light). **(c)** Irregularly shaped garnet around poikiloblastic clinopyroxene with a polycrystalline quartz inclusion (nearly cross-polarised light). **(d)** Elongated garnet and clinopyroxene with quartz inclusions (nearly cross-polarised light). **(e, f)** Elongated grain shapes defining a foliation (**e** – in plane-polarised light, **f** – in nearly cross-polarised light). Cpx(L), clinopyroxene with oriented lamellae. Ilm, ilmenite. Other mineral abbreviations are as in Table 1.

four samples with few secondary minerals have homogeneous grain cores with low Al_2O_3 contents in the range of 0.17 wt %–0.37 wt % (Fig. 8a, b, d, e). These low values increase gradually towards grain rims to maximal values between ∼ 1 wt % and ∼ 2 wt %. Other oxides show little variation in their contents. Grains of much smaller grain size lack plateaus of low Al_2O_3 contents. Millimetre-size grains in the Langeneset sample, which is rich in secondary minerals, have abundant Al_2O_3 that either increases from cores (∼ 1.5 wt %) to rims (∼ 2 wt %) or occurs at rim values throughout the grain (∼ 2 wt %; Fig. 8c, f). FeO contents also increase from grain cores to grain rims, whereas MgO contents show an inverse pattern.

4.3 Geothermobarometry

Metamorphic pressures and temperatures were calculated from the average mineral core compositions given in Tables 3, 4, and 6. These compositions were applied to the Al-in-orthopyroxene geobarometer of Brey and Köhler (1990), the Ca-in-orthopyroxene geothermometer of Brey and Köhler (1990), and the En-in-clinopyroxene geothermometer

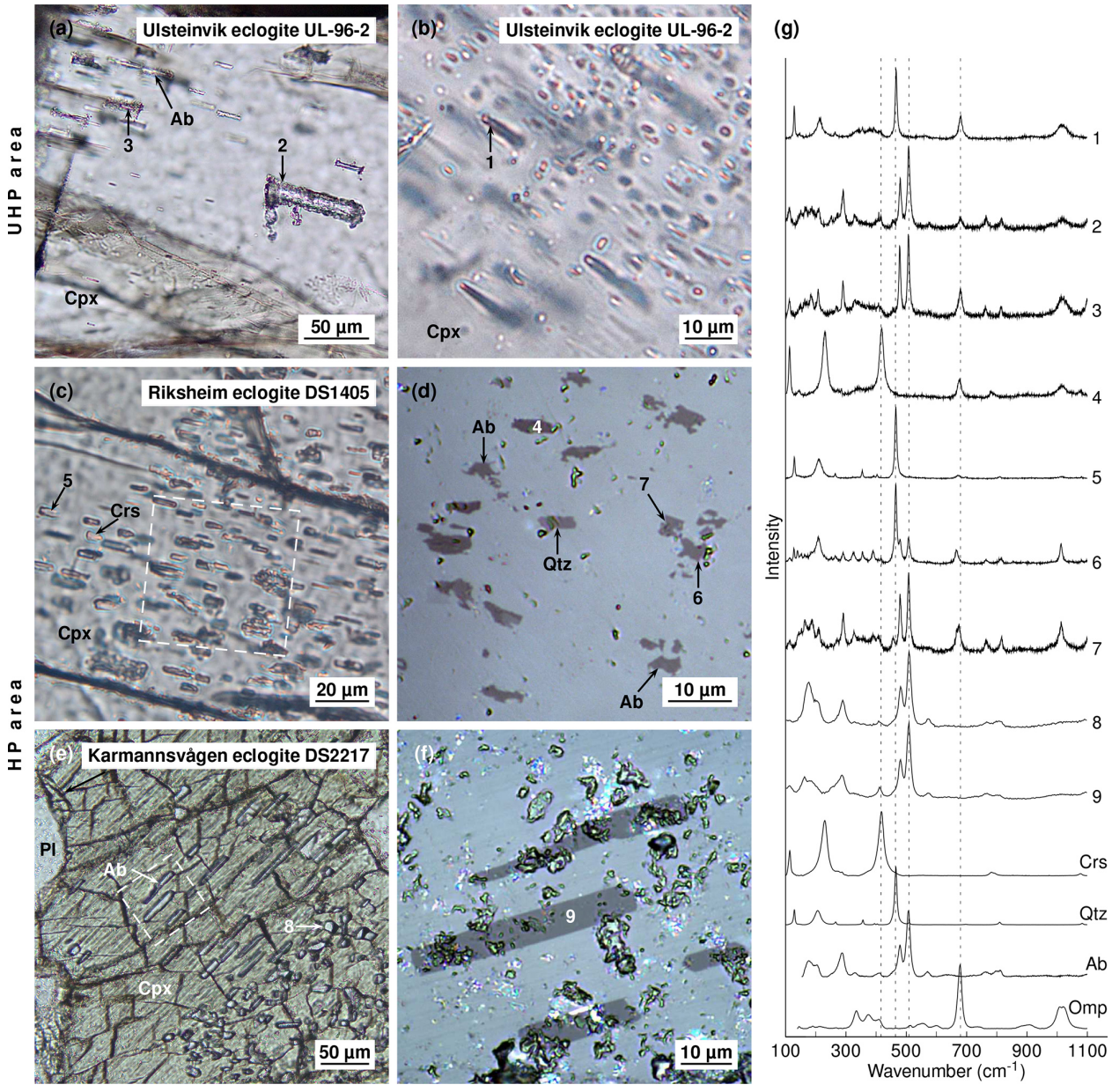

Figure 5. Oriented monomineralic inclusions in the clinopyroxenes of WGR orthopyroxene-free eclogites from HP and UHP areas and related Raman spectra. **(a–d)** Short-prismatic to needle-shaped inclusions with straight interfaces (Qtz) and irregular interfaces (Ab and α-cristobalite, Crs) with the host. **(e–f)** Lamellar to needle-shaped albite with straight interfaces with the host. Dashed squares outline magnified regions shown in adjacent panels. Panels **(a)**–**(c)** and **(e)** in plane-polarised light, **(d)** and **(f)** in reflected light. **(g)** Raman spectra (labelled) obtained at positions shown in **(a)**–**(f)**. Dashed lines show the main peak positions in the reference spectra for Crs (416 cm^{-1}), Qtz (464 cm^{-1}), Ab (508 cm^{-1}), and omphacite (Omp; 679 cm^{-1}) obtained from the RRUFF database (Lafuente et al., 2015). Speckles in **(f)** are reflections due to uneven surface polishing. Mineral abbreviations are as in Table 1.

of Nimis and Taylor (2000). Application of the latter to orthopyroxene-free eclogites required hypothetical pressures to be chosen (Table 7). The orthopyroxene-based barometer and thermometer were calibrated for a pressure range of 2.8–6.0 GPa and a temperature range of 900–1400 °C, and they reproduced experimental pressures for natural lherzolitic compositions to ±0.22 GPa (1σ) and temperatures to ±19 °C (1σ). Lherzolites have low Na contents, which also characterise many of our eclogite samples, which contain omphacitic clinopyroxene (jadeite > 20 mol %) in only four samples (Table 4; Fig. 7a). However, the barometer and thermometer of Brey and Köhler (1990) are based on the mineral chemistry of garnet and orthopyroxene, which both contain Na in trace amounts. Therefore, any influence of whole-rock

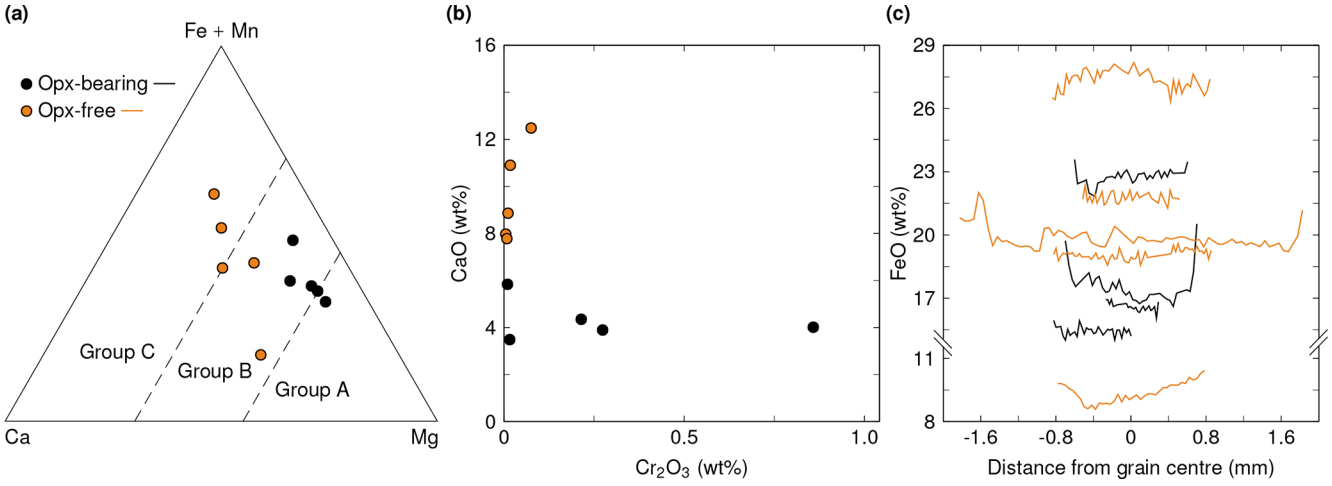

Figure 6. Mineral chemistry of garnets in WGR eclogites, subdivided according to whether the mineral assemblage is Opx-bearing or Opx-free (Opx – orthopyroxene). **(a)** Triangular diagram showing the proportions of divalent cations of average grain-core compositions. Compositional fields are from Coleman et al. (1965). **(b)** Covariation of CaO against Cr_2O_3. **(c)** FeO contents in garnet cores and rims (9 out of 10 samples).

Table 3. Garnet core average compositions (wt %).

Sample type	Opx-bearing eclogite					Opx-free eclogite				
Sample no.	M65	DS2216	DS0326	2-4A	DS1409	DS1438	DS2217	DS1405	UL-96-2	DS2204
Grain no.	#1	#4	#5	#2	#2	#1	#7	#5	#1	#6
n	*5*	*6*	*6*	*6*	*8*	*4*	*8*	*9*	*8*	*6*
SiO_2	40.9	40.5	40.5	41.5	40.1	41.6	37.9	40.1	39.8	38.5
TiO_2	0.03	0.01	0.01	0.02	0.03	0.04	0.05	0.02	0.05	0.04
Al_2O_3	22.7	23.3	22.8	23.2	22.5	23.4	21.2	22.7	22.4	22.1
Cr_2O_3	0.86	< 0.03	0.21	0.27	< 0.03	0.07	< 0.03	< 0.03	< 0.03	< 0.03
FeO	16.4	17.3	17.2	15.4	22.7	8.67	27.8	19.8	18.9	23.2
MnO	0.43	0.68	0.49	0.33	0.38	0.17	0.62	0.36	0.47	1.07
MgO	15.0	12.7	14.5	16.1	11.3	14.1	4.73	9.79	7.95	6.35
CaO	4.01	5.84	4.36	3.91	3.49	12.5	7.81	7.99	10.9	8.89
Na_2O	< 0.02	< 0.02	< 0.02	< 0.02	< 0.02	< 0.02	0.02	< 0.02	< 0.02	0.02
K_2O	< 0.01	< 0.01	< 0.01	< 0.01	< 0.01	< 0.01	< 0.01	< 0.01	< 0.01	< 0.01
Total	100.4	100.4	100.0	100.8	100.6	100.5	100.2	100.7	100.5	100.2
cations per 12 O										
Si	2.995	2.993	2.986	3.002	3.009	2.996	2.979	3.000	3.004	2.972
Ti	0.002	0.000	0.000	0.001	0.001	0.002	0.003	0.001	0.003	0.002
Al	1.963	2.026	1.982	1.983	1.990	1.991	1.967	2.001	1.991	2.011
Cr	0.050	0.001	0.012	0.016	0.001	0.004	0.000	0.000	0.001	0.001
Fe^{2+}	1.007	1.068	1.061	0.934	1.421	0.523	1.831	1.238	1.191	1.496
Mn	0.027	0.042	0.031	0.020	0.024	0.010	0.041	0.023	0.030	0.070
Mg	1.638	1.401	1.598	1.738	1.267	1.512	0.555	1.093	0.894	0.731
Ca	0.315	0.462	0.345	0.303	0.280	0.965	0.658	0.642	0.883	0.736
Na	0.000	0.000	0.000	0.001	0.000	0.001	0.003	0.001	0.002	0.003
K	0.000	0.000	0.000	0.000	0.000	0.000	0.000	0.000	0.000	0.000
Total	7.997	7.993	8.016	7.998	7.995	8.005	8.036	7.999	7.999	8.021

https://doi.org/10.5194/ejm-35-1125-2023

Table 4. Mineral core average compositions (wt %) and calculated endmembers (mol %) of clinopyroxene with oriented inclusions.

Sample type	Opx-bearing eclogite										Opx-free eclogite										
Sample no.	M65			DS2216	DS0326			2-4A	DS1409		DS1438		DS2217		DS1405		UL-96-2		DS2204		
Grain no.	#2	#3	#4	#6	#6	#9	#21	#8	#7	#8	#1	#4	#1	#6	#2	#5	#2	#4	#1	#2	#5
n	*5*	*14*	*8*	*5*	*8*	*5*	*6*	*6*	*8*	*9*	*6*	*8*	*5*	*10*	*9*	*10*	*6*	*6*	*10*	*10*	*10*
SiO_2	55.2	54.5	55.3	53.5	54.1	54.5	54.0	55.0	55.2	55.1	54.8	54.8	51.2	51.7	53.9	54.1	55.6	56.1	54.1	54.5	54.4
TiO_2	0.09	0.04	0.07	0.14	0.05	0.03	0.06	0.03	0.11	0.10	0.07	0.06	0.21	0.16	0.20	0.16	0.13	0.10	0.02	0.02	0.03
Al_2O_3	5.73	5.08	4.38	2.98	1.91	2.48	2.03	2.35	6.15	6.29	6.35	5.93	2.62	2.43	9.92	10.5	12.4	12.6	2.56	2.66	2.58
Cr_2O_3	0.74	0.61	0.45	0.80	0.20	0.21	0.20	0.15	0.03	0.03	0.05	0.03	< 0.03	< 0.03	0.03	0.04	< 0.03	< 0.03	< 0.03	< 0.03	< 0.03
FeO	3.49	3.52	3.74	5.03	7.07	6.92	7.20	2.82	6.70	6.80	1.55	1.52	11.4	11.0	4.65	4.70	3.08	3.10	5.07	5.28	5.05
MnO	0.05	0.06	0.06	0.08	0.05	0.05	0.06	0.02	0.04	0.05	0.01	0.01	0.10	0.12	0.03	0.04	0.02	0.02	0.07	0.06	0.07
MgO	13.2	13.9	14.0	14.5	13.6	13.3	13.6	15.7	11.2	11.1	14.4	14.6	11.6	11.8	10.4	10.0	8.62	8.48	14.3	14.1	14.4
CaO	17.9	19.7	19.1	21.3	19.4	19.0	19.4	21.6	15.7	15.6	21.1	21.3	21.0	20.8	16.9	16.2	13.7	13.2	21.3	21.0	21.2
Na_2O	3.44	2.44	2.78	1.36	2.65	2.90	2.64	1.61	4.53	4.50	2.14	1.99	0.94	1.09	4.18	4.49	6.58	6.89	1.84	2.10	1.81
K_2O	< 0.01	0.01	0.01	0.01	< 0.01	< 0.01	< 0.01	< 0.01	< 0.01	0.01	< 0.01	0.01	0.01	0.02	< 0.01	< 0.01	< 0.01	< 0.01	0.02	< 0.01	< 0.01
Total	99.8	99.9	99.9	99.7	99.1	99.4	99.2	99.4	99.6	99.5	100.5	100.3	99.2	99.1	100.2	100.3	100.1	100.6	99.3	99.7	99.5
cations per 6 O																					
Si	1.987	1.970	1.996	1.961	1.991	1.996	1.982	1.999	1.997	1.996	1.952	1.958	1.938	1.951	1.934	1.937	1.966	1.971	1.982	1.988	1.987
Ti	0.003	0.001	0.002	0.004	0.001	0.001	0.002	0.001	0.003	0.003	0.002	0.002	0.006	0.005	0.005	0.004	0.003	0.003	0.001	0.001	0.001
Al	0.243	0.216	0.186	0.129	0.083	0.107	0.088	0.101	0.263	0.269	0.266	0.250	0.117	0.108	0.419	0.443	0.515	0.524	0.111	0.115	0.111
Cr	0.021	0.017	0.013	0.023	0.006	0.006	0.006	0.004	0.001	0.001	0.001	0.001	0.000	0.001	0.001	0.001	0.001	0.001	0.000	0.000	0.000
Fe^{3+}	0.000	0.000	0.000	0.017	0.115	0.099	0.128	0.009	0.055	0.050	0.000	0.000	0.057	0.062	0.000	0.000	0.000	0.000	0.057	0.056	0.046
Fe^{2+}	0.105	0.106	0.113	0.138	0.102	0.112	0.093	0.077	0.148	0.157	0.046	0.045	0.305	0.285	0.140	0.141	0.091	0.091	0.099	0.105	0.108
Mn	0.001	0.002	0.002	0.003	0.001	0.002	0.002	0.001	0.001	0.002	0.000	0.000	0.003	0.004	0.001	0.001	0.001	0.001	0.002	0.002	0.002
Mg	0.707	0.749	0.754	0.792	0.746	0.725	0.747	0.852	0.606	0.599	0.762	0.775	0.655	0.663	0.556	0.535	0.454	0.444	0.782	0.765	0.784
Ca	0.690	0.764	0.738	0.837	0.765	0.746	0.764	0.843	0.608	0.607	0.807	0.816	0.852	0.841	0.649	0.619	0.517	0.496	0.836	0.820	0.830
Na	0.240	0.171	0.195	0.097	0.189	0.206	0.188	0.114	0.318	0.316	0.148	0.138	0.069	0.080	0.291	0.311	0.450	0.469	0.131	0.148	0.128
K	0.000	0.000	0.000	0.000	0.000	0.000	0.000	0.000	0.000	0.000	0.000	0.000	0.000	0.001	0.000	0.000	0.000	0.000	0.001	0.000	0.000
Total	3.998	3.997	4.000	4.000	4.000	4.000	4.000	4.000	4.000	3.999	3.986	3.984	4.004	4.000	3.996	3.992	3.998	3.999	4.000	4.000	3.998
endmembers																					
CaEs	0.3	0.5	0.1	0.0	0.0	0.0	0.0	0.0	0.1	0.1	2.9	3.1	0.0	0.0	0.8	1.5	0.4	0.3	0.0	0.0	0.4
CaTs	1.3	3.0	0.4	3.9	0.9	0.4	1.8	0.1	0.3	0.4	4.8	4.2	5.8	4.9	6.6	6.3	3.4	2.9	1.8	1.2	1.3
Ti-Cpx	0.5	0.2	0.4	0.8	0.3	0.2	0.4	0.2	0.6	0.6	0.4	0.3	1.2	0.9	1.1	0.8	0.7	0.5	0.1	0.1	0.2
K-Cpx	0.0	0.0	0.0	0.0	0.0	0.0	0.0	0.0	0.0	0.0	0.0	0.0	0.0	0.1	0.0	0.0	0.0	0.0	0.1	0.0	0.0
Kos	2.1	1.7	1.3	2.3	0.6	0.6	0.6	0.4	0.1	0.1	0.1	0.1	0.0	0.1	0.1	0.1	0.1	0.1	0.0	0.0	0.0
Jd	21.4	15.1	17.8	4.9	6.5	9.9	5.1	9.9	25.6	26.0	14.3	13.3	0.0	0.8	27.9	30.2	44.3	46.3	7.3	9.1	8.0
Ae	0.0	0.0	0.0	1.7	11.5	9.9	12.8	0.9	5.5	5.0	0.0	0.0	5.7	6.2	0.0	0.0	0.0	0.0	5.7	5.6	4.6
Jhn	0.1	0.2	0.2	0.3	0.1	0.2	0.2	0.1	0.1	0.2	0.0	0.0	0.3	0.4	0.1	0.1	0.1	0.1	0.2	0.2	0.2
En	35.3	37.4	37.7	39.5	37.3	36.2	37.3	42.6	30.2	29.9	38.1	38.7	32.6	33.0	27.7	26.6	22.6	22.1	39.1	38.2	39.2
Fs	5.2	5.3	5.6	6.8	5.1	5.6	4.6	3.8	7.3	7.8	2.3	2.2	15.1	14.1	6.8	6.9	4.5	4.5	4.9	5.2	5.4
Wo	33.7	36.5	36.6	39.8	37.7	37.0	37.2	42.0	30.2	30.1	37.2	37.9	39.5	39.4	28.9	27.4	24.0	23.2	40.8	40.3	40.6
Total	100.0	100.0	100.0	100.0	100.0	100.0	100.0	100.0	100.0	100.0	100.0	100.0	100.3	100.0	100.0	100.0	100.0	100.0	100.0	100.0	100.0

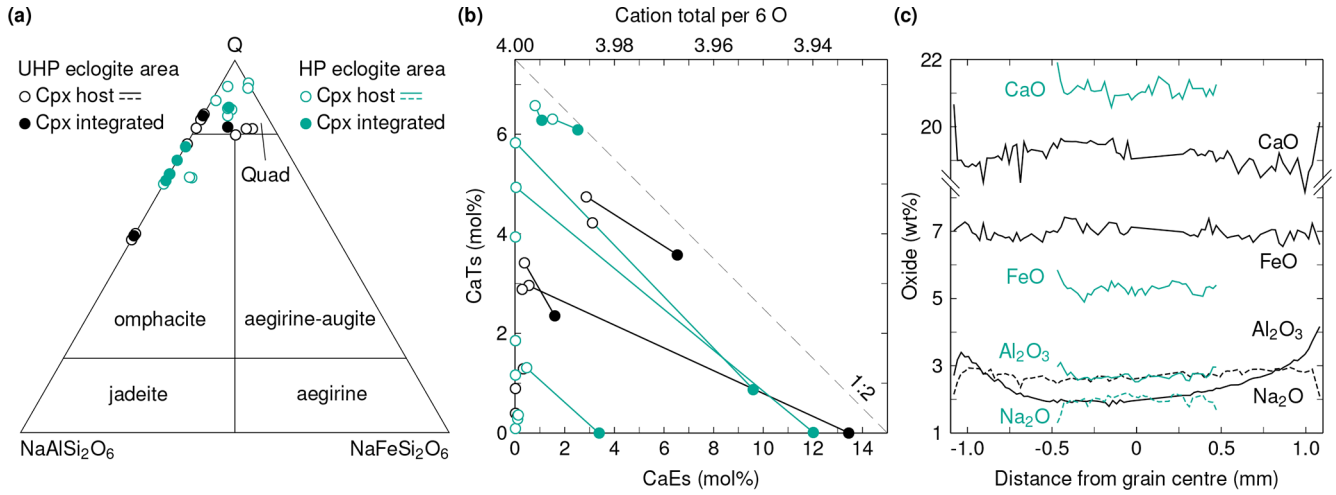

Figure 7. Mineral chemistry of clinopyroxenes (Cpx) with oriented inclusions in WGR eclogites subdivided according to sample occurrence. **(a)** Triangular diagram showing the proportions of quadrilateral (Q = Wo + En + Fs) and Na-pyroxene components after Morimoto et al. (1988). **(b)** Inverse covariance of CaTs against CaEs components in grains that contain parallel inclusions of quartz ± pargasite or albite. Solid lines connect compositions from individual grains. The slope of the dashed line refers to compositions expected for the reactions 2 CaEs → CaTs + 3 Qtz and 2 CaEs + 3 Jd → CaTs + 3 Ab (Reactions 1 and 2 in the text, respectively). **(c)** Variations in the contents of selected oxides with monovalent, divalent, and trivalent cations, as measured in grain cross-sections (long profile – sample DS0326; short profile – sample DS2204).

Na contents on calculated pressures and temperatures is regarded as negligible. The En-in-clinopyroxene thermometer was calibrated for 2.0–6.0 GPa and 850–1500 °C and reproduced experimental temperatures to ±30 °C (1σ). This calibration covered a wide range of lherzolitic compositions and included corrections for minor components, such as Na and Ti.

Four eclogites that contain orthopyroxene but few secondary minerals yielded metamorphic P–T estimates within narrow ranges (Fig. 9) of approximately 4.1–5.2 GPa and 800–850 °C if orthopyroxene was used for the temperature calculation, or approximately 3.7–5.5 GPa and 770–850 °C if clinopyroxene was used. The ranges have large overlaps in pressure and temperature. Estimates obtained using the mineral chemistry of the orthopyroxene-bearing eclogite sample from Langeneset that is rich in secondary minerals were lower in pressure (2.1–2.2 GPa) but similar in temperature (800–820 °C), irrespective of the calibration applied.

Orthopyroxene-free eclogites yielded temperatures equal to or lower than those calculated for orthopyroxene-bearing eclogites (Fig. 9). There is no systematic difference between the calculated maximum metamorphic conditions for samples from the UHP eclogite areas and those in the interjacent HP eclogite area, and there is no systematic difference between maximum metamorphic temperatures for orthopyroxene-bearing and orthopyroxene-free eclogites.

5 Discussion

5.1 Significance of eclogite type and spatial occurrence

The suite of samples can be divided into orthopyroxene-bearing and orthopyroxene-free eclogites. This subdivision has previously been addressed as "orthopyroxene-lineage" and "kyanite-lineage" eclogites (Lappin and Smith, 1981; Smith, 1988) and may be due to differences in whole-rock chemistry, which are echoed by the two trends in garnet chemistry (Fig. 6a, b). Both trends overlap those of eclogitic and pyroxenitic mantle garnets from global and regional data sets (Pearson et al., 2003; Grütter et al., 2004; Spengler et al., 2021), which may indicate different precursors for the rocks of the two sample subsets prior to their tectonic evolution. Nevertheless, samples with and without orthopyroxene occur throughout the study area without any clear spatial pattern (Fig. 1). Therefore, any difference in precursor origin does not seem to correlate with the spatial distinction of UHP and HP areas.

Retrogression in the form of chemical diffusion in minerals and the replacement of primary minerals by secondary minerals can erase part of a rock's history. Petrography and mineral chemistry indicate that this process has affected some of the studied samples. For example, the eclogites at Synes and Langeneset have similar grain size of primary minerals (several millimetres) and inclusion microstructures (irregularly shaped garnet in orthopyroxene, oriented lamellae in clinopyroxene), whereas the proportion of secondary minerals (Fig. 8a, c) and the orthopyroxene mineral chem-

Table 5. Reconstructed mineral core compositions (wt %) and calculated endmembers (mol %) from clinopyroxene with oriented inclusions.

Sample type	Opx-bearing eclogite	Opx-free eclogite						
Sample no.	M65	DS1438	DS2217		DS1405		UL-96-2	DS2204
Grain no.	#3	#1	#1	#6	#2	#5	#2	#5
area (μm^2)	*90 × 108*	*70 × 70*	*200 947*	*185 944*	*100 × 250*	*80 × 140*	*120 × 140*	*60 × 160*
SiO_2	55.5	55.0	54.2	54.8	53.5	53.5	55.6	54.0
TiO_2	0.07	0.07	0.16	0.12	0.21	0.15	0.11	0.03
Al_2O_3	5.32	6.43	7.37	8.30	9.71	10.3	12.2	2.50
Cr_2O_3	0.67	0.07	0.01	0.02	0.02	0.04	0.02	0.02
FeO	3.61	1.55	8.78	7.98	4.67	4.96	2.97	5.16
MnO	0.06	0.01	0.08	0.09	0.03	0.04	0.02	0.07
MgO	13.2	14.1	8.85	8.46	10.3	9.88	8.48	13.8
CaO	17.9	20.7	16.9	16.2	16.7	15.9	13.3	20.8
Na_2O	2.48	2.01	3.01	3.40	4.12	4.28	6.60	1.72
K_2O	0.03	0.01	0.01	0.02	0.01	0.01	0.00	0.01
Total	98.8	100.0	99.4	99.4	99.3	99.1	99.4	98.1
cations per 6 O								
Si	2.000	1.964	1.991	1.999	1.937	1.939	1.976	2.000
Ti	0.002	0.002	0.005	0.003	0.006	0.004	0.003	0.001
Al	0.226	0.270	0.319	0.357	0.414	0.439	0.512	0.109
Cr	0.019	0.002	0.000	0.000	0.001	0.001	0.001	0.000
Fe^{3+}	0.060	0.000	0.000	0.000	0.000	0.000	0.000	0.047
Fe^{2+}	0.049	0.046	0.270	0.243	0.141	0.150	0.088	0.113
Mn	0.002	0.000	0.002	0.003	0.001	0.001	0.001	0.002
Mg	0.709	0.752	0.485	0.460	0.556	0.534	0.449	0.763
Ca	0.691	0.791	0.665	0.634	0.649	0.618	0.508	0.824
Na	0.173	0.139	0.214	0.240	0.289	0.301	0.455	0.124
K	0.001	0.000	0.001	0.001	0.001	0.000	0.000	0.000
Total	3.933	3.967	3.952	3.940	3.995	3.987	3.992	3.983
endmembers								
CaEs	13.5	6.5	9.6	12.0	1.0	2.5	1.6	3.4
CaTs	0.0	3.6	0.9	0.1	6.3	6.1	2.4	0.0
Ti-Cpx	0.4	0.4	0.9	0.6	1.1	0.8	0.6	0.2
K-Cpx	0.1	0.0	0.1	0.1	0.1	0.0	0.0	0.0
Kos	1.9	0.2	0.0	0.0	0.1	0.1	0.1	0.0
Jd	9.0	13.3	20.5	23.4	27.8	29.1	44.9	7.5
Ae	6.0	0.0	0.0	0.0	0.0	0.0	0.0	4.7
Jhn	0.2	0.0	0.2	0.3	0.1	0.1	0.1	0.2
En	35.4	37.5	24.1	22.9	27.7	26.6	22.4	38.2
Fs	2.4	2.3	13.4	12.1	6.9	7.4	4.3	5.6
Wo	31.1	36.1	30.3	28.5	29.0	27.2	23.8	40.2
Total	100.0	100.0	100.0	100.0	100.0	100.0	100.0	100.0

istry (Fig. 8d, f) differ. The latter has led to estimates of metamorphic pressures for both samples to deviate by > 2 GPa (Table 7), corresponding to > 60 km of lithospheric depth. However, both samples are now exposed only 10 km apart on the same island (Fig. 1), and it follows that either (i) both eclogites are spatially unrelated in that they represent different components in a tectonic mélange, or (ii) a major tectonic structure across the island offsets rocks in the SW with metamorphism in the diamond stability field from those in the NE with metamorphism in the quartz stability field, or (iii) post-peak metamorphic diffusion obliterated the shared tectonic history from the Langeneset sample.

Explanation (iii) is supported by the coincidence of the low pressure estimate for the Langeneset sample with its high proportion of secondary minerals (i.e. high degree of alteration) and the high intensity of chemical diffusion recorded

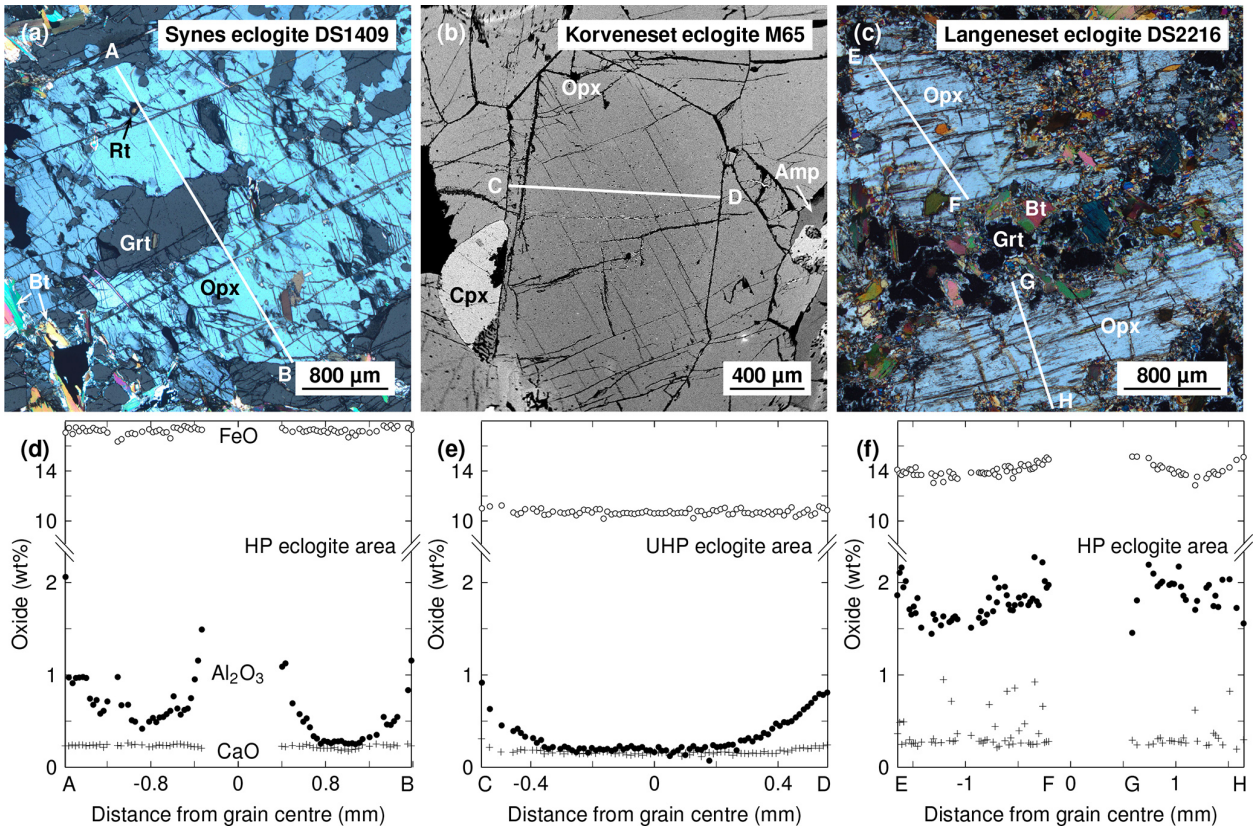

Figure 8. Variations of the contents of selected element oxides in orthopyroxene. **(a)** Irregularly shaped garnet inclusions in orthopyroxene from a sample with a low proportion of secondary minerals (nearly cross-polarised light). **(b)** Inclusion-free orthopyroxene with elongated grain shape from a sample with a low proportion of secondary minerals (back-scattered electron image). **(c)** Mineral microstructure as in **(a)**, but from a sample with high proportion of secondary minerals (cross-polarised light). **(d–f)** EMP line scans (labelled) for FeO, Al_2O_3, and CaO along profiles shown in **(a)**–**(c)**. Mineral abbreviations are as in Table 1.

by its minerals. The efficiency of intracrystalline diffusion is recorded by, for example, the Fe content. The Fe content in eclogitic orthopyroxene depends on the partitioning of Fe and Mg among associated minerals (Brey and Köhler, 1990). While the flat FeO trends across the Synes orthopyroxene provide no evidence for effective diffusion (Fig. 8d), the bell-shaped profiles of FeO content in the Langeneset orthopyroxene suggest efficient diffusion (Fig. 8f) during the period after the maximum metamorphic temperatures shared by the two samples. Similarly, the Synes orthopyroxene has steep profiles of Al_2O_3 contents at grain rims that flank compositional plateaus in grain cores, which shows that the mineral chemistry responded to changing pressures only at grain boundaries (i.e. low diffusion efficiency) during early decompression. In contrast, the Langeneset orthopyroxene has scattered variations in Al_2O_3 content throughout the crystals, which suggests a disturbance of older contents (Fig. 8f). In addition, the Synes orthopyroxene has ratios of core : rim Al_2O_3 contents of less than 1 : 4 (Fig. 8d), the preservation of which depended on sluggish diffusion during and after decompression. On the other hand, the Langeneset orthopyroxene has less extreme core : rim Al_2O_3 ratios of between 3 : 4 and unity (Fig. 8f), which are consistent with more efficient diffusion in this sample. Finally, Ca-Eskola is not known to be a stable component in clinopyroxene under the metamorphic conditions estimated from the Langeneset orthopyroxene mineral chemistry, when compared with other natural eclogites (Schmädicke and Müller, 2000). For the reasons given above, we suggest that the Langeneset sample underwent higher metamorphic conditions than indicated by its present mineral chemistry. Alternatively, if the tectonic features noted under (i) or (ii) applied, then the coincidence of differences in metamorphic pressure, sample alteration, and diffusion efficiency would be by chance. Equally by chance would be the coincidence of Ca-Tschermak : Ca-Eskola ratios of approximately 1 : 2 in clinopyroxene grains with oriented inclusions shared by the sample suite (Fig. 7b) and the clinopyroxene in Reaction (1) (see Sect. 5.2).

The orthopyroxene-free eclogites also record a retrogression that variably affected the sample suite. For example, symplectites of secondary clinopyroxene and plagioclase that vary in grain size and shape (lamellar versus granular) par-

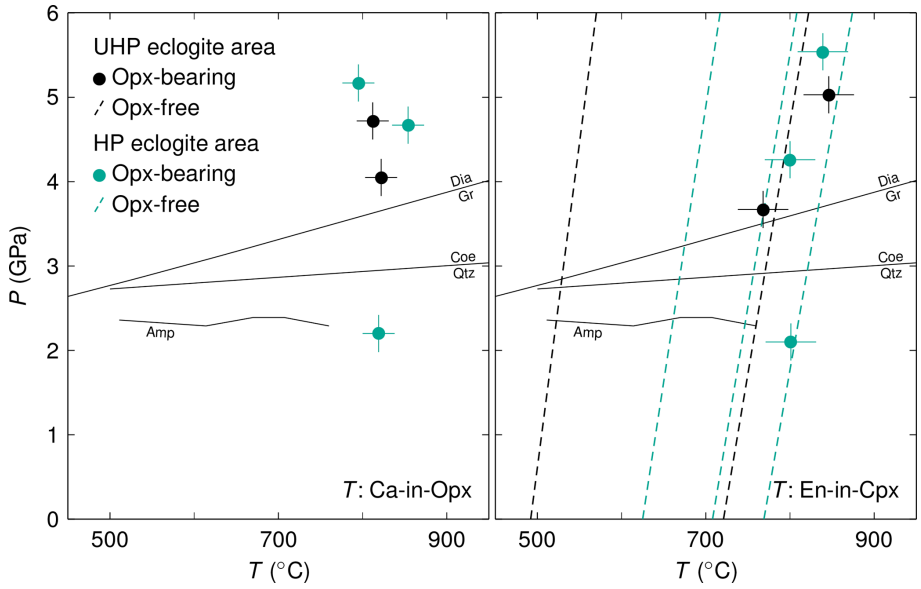

Figure 9. *P–T* diagrams showing the geothermobarometric estimates given in Table 7. Labelled lines show the phase transitions for graphite–diamond (Dia/Gr; Day, 2012), quartz–coesite (Coe/Qtz; Bose and Ganguly, 1995), and the upper stability of amphibole (Amp) in water-saturated mid-ocean ridge basalt (Schmidt and Poli, 1998). Cpx – clinopyroxene. Opx – orthopyroxene.

Table 6. Orthopyroxene core average compositions (wt %).

Sample type	Opx-bearing eclogite				
Sample no.	M65	DS2216	DS0326	2-4A	DS1409
Grain no.	#51	#2	#7	#2	#2
n	*16*	*7*	*5*	*6*	*4*
SiO_2	56.5	55.1	56.6	57.5	55.4
TiO_2	< 0.01	0.03	0.01	0.01	< 0.01
Al_2O_3	0.19	1.48	0.37	0.17	0.26
Cr_2O_3	< 0.03	0.26	0.03	0.04	< 0.03
FeO	10.7	13.2	11.0	8.81	17.0
MnO	0.09	0.20	0.11	0.07	0.09
MgO	31.5	29.0	31.3	33.1	27.1
CaO	0.14	0.27	0.18	0.12	0.18
Na_2O	0.02	< 0.02	< 0.02	< 0.02	0.02
K_2O	< 0.01	< 0.01	< 0.01	< 0.01	< 0.01
Total	99.2	99.6	99.6	99.8	100.0
cations per 6 O					
Si	1.999	1.969	1.997	2.002	2.000
Ti	0.000	0.001	0.000	0.000	0.000
Al	0.008	0.062	0.015	0.007	0.011
Cr	0.001	0.007	0.001	0.001	0.000
Fe^{2+}	0.317	0.396	0.324	0.257	0.514
Mn	0.003	0.006	0.003	0.002	0.003
Mg	1.664	1.542	1.646	1.719	1.458
Ca	0.005	0.010	0.007	0.004	0.007
Na	0.001	0.000	0.001	0.000	0.001
K	0.000	0.000	0.000	0.000	0.000
Total	3.997	3.995	3.995	3.993	3.995

tially replaced primary clinopyroxene in some samples from UHP and HP areas (Fig. 4e, f), but not in other samples (Fig. 4c). Similarly, quartz needles in clinopyroxene are replaced by albite only in some of the samples exposed in UHP and HP areas (Fig. 5a–d).

Further evidence of chemical diffusion in the minerals is preserved in the clinopyroxene of the Remøysunde eclogite. The largest grains (> 2 mm in grain size) show that elements with highly charged ions and low diffusivity, such as Al^{3+}, have oxide contents that vary from cores to inner rims by a factor of 2, while the oxide contents of lower charged ions with higher diffusivity, such as Na^{+} and Fe^{2+}, are constant from core to rim (Fig. 7c; Cherniak and Dimanov, 2010). The slope of isopleths in *P–T* space for Al in clinopyroxene implies that an increase in Al content requires either an increase in temperature or a decrease in pressure (Gasparik, 2014). The former would be expected to modify the FeO content (due to the temperature-dependent Fe–Mg distribution with associated garnet and orthopyroxene), while the latter would be expected to decrease the Na_2O content (due to the pressure-dependency of the jadeite component). As neither FeO nor Na_2O (in contrast to Al_2O_3) shows major content variations from cores to inner rims, element diffusion prior to late retrogression seems the most likely explanation. This diffusion during early retrogression may explain why the sample from the Remøysunde eclogite provides the lowest estimates of metamorphic *P–T* within the stability field of diamond (Table 7; Fig. 9).

Variable degrees of retrogression affected eclogites across the boundaries of the UHP and HP areas, and this is expected to have influenced the mineral chemistry commonly used to

Table 7. Geothermobarometric estimates using mineral compositions in Tables 3, 4, and 6 (P in GPa/T in °C, * preset P).

Sample type	Opx-bearing eclogite					Opx-free eclogite				
Sample no.	M65	DS2216	DS0326	2-4A	DS1409	DS1438	DS2217	DS1405	UL-96-2	DS2204
(1) Al-in-Opx/Ca-in-Opx, Brey and Köhler (1990)										
	4.72/812	2.20/819	4.05/822	5.17/795	4.67/854	–	–	–	–	–
(2) Al-in-Opx/En-in-Cpx, Brey and Köhler (1990)/Nimis and Taylor (2000)										
	5.03/846	2.10/801	3.67/768	5.54/839	4.26/800	2*/754 4*/788	2*/ 804 4*/ 839	2*/742 4*/775	2*/518 4*/544	2*/656 4*/686

obtain information about metamorphic conditions. A look through this retrogression history is useful for distinguishing rocks that were unaffected by UHP metamorphism and ultimately constraining the mechanisms of tectonic exhumation.

5.2 Shared eclogite-facies attributes

Poikiloblastic textures and irregular- to skeletal-shaped eclogite-facies mineral inclusions in eclogite-facies minerals (i.e. pyroxene in garnet and vice versa at the absence of plagioclase; Figs. 2a–d, 4a, and 8a) suggest a magmatic origin under eclogite-facies conditions for at least some orthopyroxene-bearing and orthopyroxene-free samples. On the other hand, the occurrence of foliation-parallel elongated eclogite-facies grains indicates their formation during the latest geodynamic event (Figs. 2e–f, 4e–f, and 8b). Both types of texture (i) can occur in single samples and even within a single thin section (Fig. 2c, e), (ii) have clinopyroxene that contains oriented inclusions including quartz (Figs. 2c, e and 3c–d), and (iii) have low-Al orthopyroxene, unless the grains have been severely altered (Fig. 8). Because a magmatic origin for the eclogites is unlikely to have post-dated the tectonic UHP metamorphism, we suggest that the mineral chemistry from the inferred magmatic stage was widely erased by mineral-chemical re-equilibration during the UHP metamorphic event. Using the same reasoning, it is unlikely that the origin of the oriented inclusions including quartz in poikiloblastic (i.e. magmatic) and elongated (i.e. tectonic) clinopyroxene grains is related to the magmatic mineralogy, and therefore the inclusions can be regarded as providing information on the UHP metamorphic stage.

The mineral microstructures inferred to be magmatic, as described above, add to those reported earlier from another WGR eclogite (located at Årsheimneset, about 1 km SE of Sandviknes), which contains lamellae of garnet in orthopyroxene and orthopyroxene in clinopyroxene that have been interpreted to be the result of exsolution from precursor minerals stable under upper-mantle conditions of 3–4 GPa and 1200–1370 °C (Lappin and Smith, 1978). Similar exsolution microstructures characterise eclogites and websterites enclosed in WGR orogenic peridotite, which suggests stability of the precursor minerals under pressures of 3.0–4.5 GPa and temperatures of 1500–1600 °C (Carswell, 1973; Lappin, 1974; Brueckner et al., 2002; van Roermund et al., 2002). The magmatic microstructures in the gneiss-hosted eclogites, the formation of precursor minerals under upper-mantle conditions, and the similar microstructures reported from mafic–ultramafic rocks enclosed in associated orogenic peridotites indicate that some of the gneiss-hosted eclogites (particularly the orthopyroxene-bearing ones) may represent fragments of the upper mantle (Lappin and Smith, 1978) that were incorporated into WGR crustal gneiss, probably together with orogenic peridotites (Brueckner, 1998). Support for this interpretation is given by the overlap in the mineral chemistry of garnets in the gneiss-hosted orthopyroxene-bearing eclogites (Fig. 6a–b) and the orogenic peridotite-hosted websterites that equilibrated under a similar pressure of 3.4 ± 4 GPa in the mantle prior to tectonism (Spengler et al., 2021).

Alternatively, it has been proposed on the basis of mineral textures, whole-rock chemistry, and multi-phase and fluid inclusion studies of eclogite-facies silicates that some WGR coarse-grained orthopyroxene-bearing eclogites and pyroxenites (Svartberget, Årsheimneset) were formed by reactions between felsic partial melts and ultramafic rocks under conditions of the graphite–diamond phase transition and beyond and possibly in association with supercritical fluids (Vrijmoed et al., 2006, 2008, 2013; Quas-Cohen, 2014; Hughes et al., 2021). The applicability of this metasomatic process to the origin of the present samples is unconstrained, but it would independently support an UHP metamorphic history for the orthopyroxene-bearing samples exposed in our HP and UHP study areas (Fig. 1).

All the investigated eclogite samples contain oriented inclusions in the primary (i.e. poikiloblastic and elongated but not symplectic) clinopyroxene. The mineralogy of these inclusions seems to depend on the eclogite mineral assemblage (i.e. the whole-rock chemistry). While orthopyroxene-bearing eclogites have needles of quartz + pargasite, the orthopyroxene-free eclogites contain (with the exception of a single sample) either quartz needles or albite lamellae depending on the proportions of matrix quartz and ilmenite (Table 1). Aligned inclusions with comparable shapes have been interpreted as having been exsolved from former solid-solution precursor minerals in a variety of solid-

solution systems, e.g. garnet/clinopyroxene/orthopyroxene–rutile, garnet–pyroxene, and olivine–$FeTiO_3$ (Griffin et al., 1971; Haggerty and Sautter, 1990; Dobrzhinetskaya et al., 1996), as well as clinopyroxene–SiO_2 (Smith and Cheeney, 1980; Smith, 1984; Shatsky et al., 1985; Bakun-Czubarow, 1992; Katayama et al., 2000; Schmädicke and Müller, 2000; Zhang et al., 2005). The formation of free silica from clinopyroxene can be explained by the following reaction:

$$2\,Ca_{0.5}\square_{0.5}AlSi_2O_6 \rightarrow CaAl_2SiO_6 + 3\,SiO_2 + \square, \quad \text{(R1)}$$

which describes the consumption of vacancies (□) in non-stoichiometric pyroxene. It follows that the mineral chemistry can be used to test whether Reaction (1) applies to some of our investigated samples.

Reconstructed compositions of clinopyroxene core areas that contain either (a) quartz + pargasite, (b) fresh quartz, (c) partially replaced quartz, or (d) albite all have non-stoichiometric compositions that translate to higher Ca-Eskola and lower Ca-Tschermak components than in the host clinopyroxene (Tables 4 and 5). Endmember proportions of individual grain compositions suggest that an exsolution origin would have increased the Ca-Tschermak component of the host grain at the expense of its Ca-Eskola component to a ratio of approximately 1 : 2 (Fig. 7b). This ratio is required for the quartz-forming Reaction (1). However, all pairs of composition of integrated and host minerals show roughly the same ratio, implying that the investigated microstructures with oriented inclusions formed similarly. The exsolution of lamellar Na-rich plagioclase, which is shown in Fig. 5e–f and which occurs also in the omphacite of an UHP eclogite from the Erzgebirge (Schmädicke and Müller, 2000), can be explained when the breakdown of jadeite is included in Reaction (1), as follows:

$$2\,Ca_{0.5}\square_{0.5}AlSi_2O_6 + 3\,NaAlSi_2O_6 \\ CaAl_2SiO_6 + 3\,NaAlSi_3O_8 + \square. \quad \text{(R2)}$$

A stepwise breakdown of first the Ca-Eskola component by Reaction (1) and subsequently the jadeite component is done by the following reaction:

$$NaAlSi_2O_6 + SiO_2 \rightarrow NaAlSi_3O_8 \quad \text{(R3)}$$

would first form quartz needles that subsequently transform to albite, a process that is suggested by the irregular inclusion–host interfaces in the samples from Riksheim and Ulsteinvik (Fig. 5a–d), as well as by the associated Al-depletion halos in the proximal host clinopyroxene (File S2).

The close intergrowth relationship of quartz + pargasite in the needles suggests that both phases formed simultaneously. With the exception of the Fjørtoftvika eclogite, these bimineralic inclusions are absent from the orthopyroxene-free samples, but they occur in all the orthopyroxene-bearing samples. This suggests that the formation of quartz needles with or without pargasite depends on the whole-rock chemistry and probably also on the hydrous content that was inherited from the precursor rocks (Terry et al., 2003) rather than on the availability of a hydrous fluid derived from an external source (Page et al., 2005). Otherwise, the observed correspondence would be by chance. Natural clinopyroxene in mantle and crustal eclogites is known to host between ~ 200 and $> 1000\,\mu g\,g^{-1}$ H_2O (Smyth et al., 1991; Bell et al., 2004; Skogby et al., 2016; Gose and Schmädicke, 2022). Moreover, clinopyroxene is the most hydrous phase in eclogitic mineral assemblages in the absence of other hydrous mineral phases (Bell and Rossman, 1992). The exsolution of 1 % pargasite with 4 wt % H_2O could have formed isochemically from a hydrous precursor clinopyroxene with $400\,\mu g\,g^{-1}$ H_2O, a value that is exceeded in many natural eclogites. Therefore, the bimineralic oriented inclusions may have, at least in theory, an isochemical origin.

Recognition that the oriented microstructures formed by exsolution implies that all the eclogites were in the stability field of the Ca-Eskola component. The stability field for non-stoichiometric clinopyroxene is disputed, but natural data sets and experimental studies point to pressure and temperature conditions beyond the stability of quartz (Katayama et al., 2000; Schmädicke and Müller, 2000; Bruno et al., 2002; Knapp et al., 2013; Schroeder-Frerkes et al., 2016), with the exception of a single experimental data point at 2.5 GPa and 850 °C (Konzett et al., 2008). These data suggest that the onset of Ca-Eskola stability is close to the quartz–coesite phase transition.

When focusing on the presented data set, the combined breakdown of Ca-Eskola and jadeite endmembers, either in a single step (Reaction 2) or in a double step (Reaction 1 followed by Reaction 3), implies a simple geodynamic scenario in which the microstructures formed during decompression. This is because of the position of the jadeite isopleths with a positive slope in pressure–temperature space. The formation of rare metastable α-cristobalite could have been associated with the formation of quartz if vacancy consumption along with dehydration applied, as has recently been proposed for epitactically exsolved α-cristobalite in omphacite from the Nové Dvory UHP eclogite, in the Bohemian Massif (Hill et al., 2019):

$$2\,Mg_{1.5}\square_{0.5}Si_2O_6H \rightarrow 1.5\,Mg_2Si_2O_6 + \square + SiO_2 + H_2O. \quad \text{(R4)}$$

The development of the oriented inclusions in the WGR eclogites is most likely to have occurred within the eclogite facies; otherwise, it is unlikely that the microstructure would be preserved in primary clinopyroxene. This leads to the question of where the decompression started.

Unless secondary processes caused strong overprints, the geothermobarometric estimates for the microstructure-bearing eclogites indicate that decompression passed through the diamond stability field for all the orthopyroxene-bearing samples from the UHP and HP areas (Fig. 9).

Orthopyroxene-free eclogites yielded overlapping temperature estimates, except for two samples from the Ulsteinvik and Årsetneset eclogites (Fig. 9b). The reasons for those two lower temperatures were not investigated further, but they could be related to a combination of the different thermometers involved in our calculations and the different degrees of retrograde overprinting that especially affected the Ulsteinvik eclogite (Carswell et al., 2003a). Most of our pressure–temperature estimates give a consistent picture of metamorphism under minimum conditions of 4.64 GPa and 817 °C (average of estimates for four orthopyroxene-bearing eclogites; Table 7) and early retrogression through 2.15 GPa and 810 °C (average of estimates from one orthopyroxene-bearing eclogite) for the Storfjord–Moldefjord region in the WGR. Similar estimates of metamorphic conditions had been published previously for other mafic and ultramafic rocks in the adjacent Gurskøy–Storfjord and Moldefjord regions (Terry et al., 2000; Spengler et al., 2009, 2021) and even earlier for the Selje area farther to the southwest (Lappin and Smith, 1978, 1981).

To summarise, the spatial extent of eclogite that experienced UHP metamorphic conditions in the WGR exceeds that of the previously recognised UHP metamorphic areas, and the UHP area should be extended to include all our investigated samples (Fig. 1). A direct implication is that the distribution of recorded or preserved metamorphic pressures in the eclogites is a function of post-peak metamorphic retrogression, and it is not necessarily significant for the reconstruction of the geometries of tectonic units (Hacker, 2007).

6 Conclusions

Our study of five orthopyroxene-bearing and five orthopyroxene-free eclogites exposed between the Storfjord and Moldefjord regions in the WGR of Norway led us to the following conclusions:

1. The mineral chemistry of orthopyroxene-bearing eclogites records a metamorphism in the diamond stability field for occurrences within and interjacent to UHP areas. Estimates of the conditions of peak metamorphism are indistinguishable from one another except where they have been obscured by retrogression.

2. All our samples have primary clinopyroxene that contains parallel inclusions of needles or lamellae that are composed of either quartz + pargasite, quartz, partially replaced quartz, or albite. The reconstructed clinopyroxene compositions are non-stoichiometric. Systematics between Ca-Eskola and Ca-Tschermak components suggest that the oriented microstructures formed by the breakdown of Ca-Eskola.

3. The breakdown of jadeite was involved in the formation of albite lamellae directly from clinopyroxene or as a result of a reaction between quartz needles and the host clinopyroxene, and this suggests that the oriented microstructures in the clinopyroxene formed during decompression.

Data availability. The Raman spectra from the RRUFF database were retrieved for reference on the project's publicly accessible website (https://rruff.info, last access: 31 March 2023).

Supplement. The supplement related to this article is available online at: https://doi.org/10.5194/ejm-35-1125-2023-supplement.

Author contributions. DS and SJC provided the samples. DS was responsible for the initial concept, wrote the initial manuscript, drew the figures, and performed the calculations. AW carried out the EMPA work. XZ and AL introduced DS to Raman spectroscopy. All authors discussed the data and contributed to the final version of the manuscript.

Competing interests. The contact author has declared that none of the authors has any competing interests.

Disclaimer. Publisher's note: Copernicus Publications remains neutral with regard to jurisdictional claims made in the text, published maps, institutional affiliations, or any other geographical representation in this paper. While Copernicus Publications makes every effort to include appropriate place names, the final responsibility lies with the authors.

Special issue statement. This article is part of the special issue "(Ultra)high-pressure metamorphism, from crystal to orogenic scale". It is a result of the 14th International Eclogite Conference (IEC-14) held in Paris and Lyon, France, 10–13 July 2022.

Acknowledgements. The authors gratefully acknowledge reviews by David Smith and Andrey Korsakov that led to improvements in the manuscript.

Financial support. This study received funding from Norway Grants 2014–2021 operated by the National Science Centre (Poland) under project contract no. 2020/37/K/ST10/02784 granted to Dirk Spengler.

Review statement. This paper was edited by Samuel Angiboust and reviewed by Andrey Korsakov and David Smith.

References

Bakun-Czubarow, N.: Quartz pseudomorphs after coesite and quartz exsolutions in eclogitic ompjacites of the Złote Mountains in the Sudetes (SW Poland), Archiwum mineralogiczne, 48, 3–25, 1992.

Bell, D. R. and Rossman, G. R.: Water in Earth's mantle: the role of nominally anhydrous minerals, Science, 255, 1391–1397, https://doi.org/10.1126/science.255.5050.1391, 1992.

Bell, D. R., Rossman, G. R., and Moore, R. O.: Abundance and partitioning of OH in a high-pressure magmatic system: megacrysts from the Monastery kimberlite, South Africa, J. Petrol., 45, 1539–1564, https://doi.org/10.1093/petrology/egh015, 2004.

Bose, K. and Ganguly, J.: Quartz-coesite transition revisited: reversed experimental determination at 500–1200 °C and retrieved thermochemical properties, Am. Mineral., 80, 231–238, 1995.

Brey, G. P. and Köhler, T.: Geothermobarometry in four-phase lherzolites II. New thermobarometers, and practical assessment of existing thermobarometers, J. Petrol., 31, 1353–1378, 1990.

Brown, M.: Metamorphic conditions in orogenic belts: a record of secular change, Int. Geol. Rev., 49, 193–234, https://doi.org/10.2747/0020-6814.49.3.193, 2007.

Brueckner, H. K.: Sinking intrusion model for the emplacement of garnet-bearing peridotites into continent collision orogens, Geology, 26, 631–634, https://doi.org/10.1130/0091-7613(1998)026<0631:SIMFTE>2.3.CO;2, 1998.

Brueckner, H. K., Carswell, D. A., and Griffin, W. L.: Paleozoic diamonds within a Precambrian peridotite lens in UHP gneisses of the Norwegian Caledonides, Earth Planet. Sc. Lett., 203, 805–816, 2002.

Bruno, M., Compagnoni, R., Hirajima, T., and Rubbo, M.: Jadeite with the Ca-Eskola molecule from an ultra-high pressure metagranodiorite, Dora-Maira Massif, Western Alps, Contrib. Mineral. Petr., 142, 515–519, https://doi.org/10.1007/s004100100307, 2002.

Carswell, D. A.: Garnet pyroxenite lens within Ugelvik layered garnet peridotite, Earth Planet. Sc. Lett., 20, 347–352, 1973.

Carswell, D. A., Krogh, E. J., and Griffin, W. L.: Norwegion orthopyroxene eclogites: calculated equilibration conditions and petrogenetic implications, in: The Caledonide orogen – Scandinavia and related areas, edited by: Gee, D. G. and Sturt, B. A., 823–841, John Wiley & Sons, Chichester, ISBN: 0-471-90822-3, 1985.

Carswell, D. A., Brueckner, H. K., Cuthbert, S. J., Mehta, K., and O'Brien, P. J.: The timing of stabilisation and the exhumation rate for ultra-high pressure rocks in the Western Gneiss Region of Norway, J. Metamorph. Geol., 21, 601–612, 2003a.

Carswell, D. A., Tucker, R. D., O'Brien, P. J., and Krogh, T. E.: Coesite micro-inclusions and the U/Pb age of zircons from the Hareidland Eclogite in the Western Gneiss Region of Norway, Lithos, 67, 181–190, https://doi.org/10.1016/S0024-4937(03)00014-8, 2003b.

Carswell, D. A., van Roermund, H. L. M., and Wiggers de Vries, D. F.: Scandian ultrahigh-pressure metamorphism of Proterozoic basement rocks on Fjørtoft and Otrøy, Western Gneiss Region, Norway, Int. Geol. Rev., 48, 957–977, https://doi.org/10.2747/0020-6814.48.11.957, 2006.

Cherniak, D. J. and Dimanov, A.: Diffusion in pyroxene, mica and amphibole, Rev. Mineral. Geochem., 72, 641–690, https://doi.org/10.2138/rmg.2010.72.14, 2010.

Cherniak, D. J. and Liang, Y.: Calcium diffusion in enstatite, with application to closure temperature of the Ca-in-opx thermometer, Geochim. Cosmochim. Ac., 332, 124–137, https://doi.org/10.1016/j.gca.2022.06.018, 2022.

Chin, E. J., Lee, C.-T. A., and Blichert-Toft, J.: Growth of upper plate lithosphere controls tempo of arc magmatism: constraints from Al-diffusion kinetics and coupled Lu-Hf and Sm-Nd chronology, Geochemical Perspectives Letters, 1, 20–32, https://doi.org/10.7185/geochemlet.1503, 2015.

Chopin, C.: Coesite and pure pyrope in high-grade blueschists of the Western Alps: a first record and some consequences, Contrib. Mineral. Petr., 86, 107–118, 1984.

Coleman, R. G., Lee, D. E., Beatty, L. B., and Brannock, W. W.: Eclogites and eclogites: their differences and similarities, Geol. Soc. Am. Bull., 76, 483–508, https://doi.org/10.1130/0016-7606(1965)76[483:EAETDA]2.0.CO;2, 1965.

Cuthbert, S. J., Carswell, D. A., Krogh-Ravna, E. J., and Wain, A.: Eclogites and eclogites in the Western Gneiss Region, Norwegian Caledonides, Lithos, 52, 165–195, 2000.

Day, H. W.: A revised diamond-graphite transition curve, Am. Mineral., 97, 52–62, https://doi.org/10.2138/am.2011.3763, 2012.

Dobretsov, N. L., Sobolev, N. V., Shatsky, V. S., Coleman, R. G., and Ernst, W. G.: Geotectonic evolution of diamondiferous paragneisses, Kokchetav Complex, northern Kazakhstan: The geologic enigma of ultrahigh-pressure crustal rocks within a Paleozoic foldbelt, Isl. Arc, 4, 267–279, https://doi.org/10.1111/j.1440-1738.1995.tb00149.x, 1995.

Dobrzhinetskaya, L. F., Eide, E. A., Larsen, R. B., Sturt, B. A., Trønnes, R. G., Smith, D. C., Taylor, W. R., and Posukhova, T. V.: Microdiamond in high-grade metamorphic rocks from the Western Gneiss region, Norway, Geology, 23, 597–600, https://doi.org/10.1130/0091-7613(1995)023<0597:MIHGMR>2.3.CO;2, 1995.

Dobrzhinetskaya, L. F., Green II, H. W., and Wang, S.: Alpe Arami: a peridotite massif from depth of more than 300 kilometers, Science, 271, 1841–1845, https://doi.org/10.1126/science.271.5257.1841, 1996.

Duretz, T., Gerya, T. V., Kaus, B. J. P., and Andersen, T. B.: Thermomechanical modeling of slab eduction, J. Geophys. Res., 117, B08411, https://doi.org/10.1029/2012JB009137, 2012.

Gasparik, T.: Phase Diagrams for Geoscientists – An Atlas of the Earth's Interior, 2nd Edn., Springer, https://doi.org/10.1007/978-1-4614-5776-3, 2014.

Gee, D. G., Kumpulainen, R., Roberts, D., Stephens, M. B., Thon, A., and Zachrisson, E.: Scandinavian Tectonostratigraphic Map, Sveriges Geologiska Undersökning Serie Ba, 1985.

Gee, D. G., Janák, M., Majka, J., Robinson, P., and van Roermund, H.: Subduction along and within the Baltoscandian margin during closing of the Iapetus Ocean and Baltica-Laurentia collision, Lithosphere, 5, 169–178, https://doi.org/10.1130/L220.1, 2013.

Gerya, T. V., Perchuk, L. L., and Burg, J.-P.: Transient hot channels: perpetrating and regurgitating ultrahigh-pressure, high-temperature crust–mantle associations in collision belts, Lithos, 103, 236–256, https://doi.org/10.1016/j.lithos.2007.09.017, 2008.

Gose, J. and Schmädicke, E.: H_2O in omphacite of quartz and coesite eclogite from Erzgebirge and Fichtelgebirge, Germany, J. Metamorph. Geol., 40, 665–686, https://doi.org/10.1111/jmg.12642, 2022.

Griffin, W. L. and Brueckner, H. K.: Caledonian Sm-Nd ages and a crustal origin for Norwegian eclogites, Nature, 285, 319–321, 1980.

Griffin, W. L., Jensen, B. B., and Misra, S. N.: Anomalously elongated rutile in eclogite-facies pyroxene and garnet, Norsk Geol. Tidsskr., 51, 177–185, 1971.

Griffin, W. L., Austrheim, H., Brastad, K., Bryhni, I., Krill, A. G., Krogh, E. J., Mørk, M. B. E., Qvale, H., and Tørudbakken, B.: High-pressure metamorphism in the Scandinavian Caledonides, in: The Caledonide orogen – Scandinavia and related areas, edited by: Gee, D. G. and Sturt, B. A., 783–801, John Wiley & Sons, Chichester, ISBN: 0-471-90822-3, 1985.

Grønlie, G., Mysen, B., and Bech, O. M.: Gravity investigation of the Hareidlandet eclogite, western Norway, Norsk Geol. Tidsskr., 52, 305–311, 1972.

Grütter, H. S., Gurney, J. J., Menzies, A. H., and Winter, F.: An updated classification scheme for mantle-derived garnet, for use by diamond explorers, Lithos, 77, 841–857, https://doi.org/10.1016/j.lithos.2004.04.012, 2004.

Hacker, B.: Ascent of the ultrahigh-presssure Western Gneiss Region, Norway, in: Convergent Margin Terranes and Associated Regions: A Tribute to W.G. Ernst, edited by: Cloos, M., Carlson, W. D., Gilbert, M. C., Liou, J. G., and Sorensen, S. S., Geological Society of America Special Paper 419, 171–184, Geological Society of America, https://doi.org/10.1130/2006.2419(09), 2007.

Hacker, B. R., Andersen, T. B., Johnston, S., Kylander–Clark, A. R. C., Peterman, E. M., Walsh, E. O., and Young, D.: High-temperature deformation during continental-margin subduction & exhumation: the ultrahigh-pressure Western Gneiss Region of Norway, Tectonophysics, 480, 149–171, https://doi.org/10.1016/j.tecto.2009.08.012, 2010.

Haggerty, S. E. and Sautter, V.: Ultradeep (greater than 300 kilometers), ultramafic upper mantle xenoliths, Science, 248, 993–996, https://doi.org/10.1126/science.248.4958.993, 1990.

Hill, T. R., Konishi, H., Hobbs, F., Lee, S., and Xu, H.: Precipitates of α-cristobalite and silicate glass in UHP clinopyroxene from a Bohemian Massif eclogite, Am. Mineral., 104, 1402–1415, https://doi.org/10.2138/am-2019-6773, 2019.

Hughes, L., Cuthbert, S., Quas-Cohen, A., Ruzié-Hamilton, L., Pawley, A., Droop, G., Lyon, I., Tartèse, R., and Burgess, R.: Halogens in eclogite facies minerals from the Western Gneiss Region, Norway, Minerals, 11, 760, https://doi.org/10.3390/min11070760, 2021.

Katayama, I., Parkinson, C. D., Okamoto, K., Nakajima, Y., and Maruyama, S.: Supersilicic clinopyroxene and silica exsolution in UHPM eclogite and pelitic gneiss from the Kokchetav massif, Kazakhstan, Am. Mineral., 85, 1368–1374, 2000.

Knapp, N., Woodland, A. B., and Klimm, K.: Experimental constraints in the CMAS system on the Ca-Eskola content of eclogitic clinopyroxene, Eur. J. Mineral., 25, 579–596, https://doi.org/10.1127/0935-1221/2013/0025-2326, 2013.

Konzett, J., Frost, D. J., Proyer, A., and Ulmer, P.: The Ca-Eskola component in eclogitic clinopyroxene as a function of pressure, temperature and bulk composition: an experimental study to 15 GPa with possible implications for the formation of oriented SiO_2-inclusions in omphacite, Contrib. Mineral. Petr., 155, 215–228, https://doi.org/10.1007/s00410-007-0238-0, 2008.

Krill, A. G.: Tectonics of the Oppdal area, central Norway, Geologiska Föreningen i Stockholm Förhandlingar, 102, 523–530, https://doi.org/10.1080/11035898009454505, 1980.

Krogh, E. J.: Evidence of Precambrian continent–continent collision in Western Norway, Nature, 267, 17–19, https://doi.org/10.1038/267017a0, 1977.

Kullerud, L., Tørudbakken, B. O., and Ilebekk, S.: A compilation of radiometric age determinations from the Western Gneiss Region, south Norway, Norg. Geol. Unders. B., 406, 17–42, 1986.

Kylander-Clark, A. R. C., Hacker, B. R., Johnson, C. M., Beard, B. L., Mahlen, N. J., and Lapen, T. J.: Coupled Lu–Hf and Sm–Nd geochronology constrains prograde and exhumation histories of high- and ultrahigh-pressure eclogites from western Norway, Chem. Geol., 242, 137–154, https://doi.org/10.1016/j.chemgeo.2007.03.006, 2007.

Kylander-Clark, A. R. C., Hacker, B. R., and Mattinson, C. G.: Size and exhumation rate of ultrahigh-pressure terranes linked to orogenic stage, Earth Planet. Sc. Lett., 321–322, 115–120, https://doi.org/10.1016/j.epsl.2011.12.036, 2012.

Lafuente, B., Downs, R. T., Yang, H., and Stone, N.: The power of databases: The RRUFF project, in: Highlights in Mineralogical Crystallography, edited by: Armbruster, T. and Danisi, R. M., 1–29, De Gruyter, https://doi.org/10.1515/9783110417104-003, 2015.

Lappin, M. A.: Eclogites from the Sunndal–Grubse ultramafic mass, Almklovdalen, Norway and the T–P history of the Almklovdalen masses, J. Petrol., 15, 567–601, https://doi.org/10.1093/petrology/15.3.567, 1974.

Lappin, M. A. and Smith, D. C.: Mantle-equilibrated orthopyroxene eclogite pods from the basal gneisses in the Selje district, western Norway, J. Petrol., 19, 530–584, 1978.

Lappin, M. A. and Smith, D. C.: Carbonate, silicate and fluid relationships in eclogites, Selje district and environs, SW Norway, T. Roy. Soc. Edin.-Earth, 72, 171–193, https://doi.org/10.1017/S0263593300009986, 1981.

Liu, P. and Massonne, H.-J.: An anticlockwise P–T–t path at high-pressure, high-temperature conditions for a migmatitic gneiss from the island of Fjørtoft, Western Gneiss Region, Norway, indicates two burial events during the Caledonian orogeny, J. Metamorph. Geol., 37, 567–588, https://doi.org/10.1111/jmg.12476, 2019.

March, S., Hand, M., Tamblyn, R., Carvalho, B. B., and Clark, C.: A diachronous record of metamorphism in metapelites of the Western Gneiss Region, Norway, J. Metamorph. Geol., 40, 1121–1158, https://doi.org/10.1111/jmg.12660, 2022.

Morimoto, N., Fabries, J., Ferguson, A. K., Ginzburg, I. V., Ross, M., Seifert, F. A., Zussman, J., Aoki, K., and Gottardi, G.: Nomenclature of pyroxenes, Am. Mineral., 73, 1123–1133, 1988.

Mysen, B. O. and Heier, K. S.: Petrogenesis of eclogites in high grade metamorphic gneisses, exemplified by the Hareidland Eclogite, western Norway, Contrib. Mineral. Petr., 36, 73–94, 1972.

Nimis, P. and Taylor, W. R.: Single clinopyroxene thermobarometry for garnet peridotites. Part I. Calibration and testing of a Cr–in–Cpx barometer and an enstatite–in–Cpx thermometer, Contrib. Mineral. Petr., 139, 541–554, 2000.

Page, F. Z., Essene, E. J., and Mukasa, S. B.: Quartz exsolution in clinopyroxene is not proof of ultrahigh pres-

sures: evidence from eclogites from the Eastern Blue Ridge, Southern Appalachians, U.S.A., Am. Mineral., 90, 1092–1099, https://doi.org/10.2138/am.2005.1761, 2005.

Pearson, D. G., Canil, D., and Shirey, S. B.: Mantle samples included in volcanic rocks: xenoliths and diamonds, in Treatise on Geochemistry, Volume 2: The Core and Mantle, edited by: Holland, H. D., and Turekian, K. K., 171–275, Elsevier, Oxford, https://doi.org/10.1016/B0-08-043751-6/02005-3, 2003.

Quas-Cohen, A.: Norwegian orthopyroxene eclogites: petrogenesis and implications for metasomatism and crust-mantle interactions during subduction of continental crust, PhD thesis, University of Manchester, https://research.manchester.ac.uk/en/ (last access: 20 October 2020), 2014.

Robinson, P., Terry, M. P., Carswell, T., Van Roermund, H., Krogh, T. E., Root, D., Tucker, R. D., and Solli, A.: Tectono-stratigraphic setting, structure and petrology of HP and UHP metamorphic rocks and garnet peridotites in the Western Gneiss Region, Møre and Romsdal, Norway, Tech. Rep. report no: 2003.057, Norges geologiske undersøkelse, Trondheim, Alice Wain Memorial West Norway Eclogite Field Symposium, guidebook for post-meeting field excursion, 2003.

Root, D. B., Hacker, B. R., Gans, P. B., Ducea, M. N., Eide, E. A., and Mosenfelder, J. L.: Discrete ultrahigh-pressure domains in the Western Gneiss Region, Norway: implications for formation and exhumation, J. Metamorph. Geol., 23, 45–61, https://doi.org/10.1111/j.1525-1314.2005.00561.x, 2005.

Schmidt, M. W. and Poli, S.: Experimentally based water budgets for dehydrating slabs and consequences for arc magma generation, Earth Planet. Sc. Lett., 163, 361–379, 1998.

Schmädicke, E. and Müller, W. F.: Unusual exsolution phenomena in omphacite and partial replacement of phengite by phlogopite + kyanite in an eclogite from the Erzgebirge, Contrib. Mineral. Petr., 139, 629–642, https://doi.org/10.1007/s004100000161, 2000.

Schönig, J., Meinhold, G., von Eynatten, H., and Lünsdorf, N. K.: Tracing ultrahigh-pressure metamorphism at the catchment scale, Sci. Rep., 8, 2931, https://doi.org/10.1038/s41598-018-21262-8, 2018.

Schroeder-Frerkes, F., Woodland, A. B., Uenver-Thiele, L., Klimm, K., and Knapp, N.: Ca-Eskola incorporation in clinopyroxene: limitations and petrological implications for eclogites and related rocks, Contrib. Mineral. Petr., 171, 101, https://doi.org/10.1007/s00410-016-1311-3, 2016.

Shatsky, V. S., Sobolev, N. V., and Stenina, N. G.: Structural peculiarities of pyroxenes from eclogites, Terra Cognita, 5, 436–437, 1985.

Skogby, H., Janák, M., and Broska, I.: Water incorporation in omphacite: concentrations and compositional relations in ultrahigh-pressure eclogites from Pohorje, Eastern Alps, Eur. J. Mineral., 28, 631–639, https://doi.org/10.1127/ejm/2016/0028-2533, 2016.

Smith, D. C.: Coesite in clinopyroxene in the Caledonides and its implications for geodynamics, Nature, 310, 641–644, https://doi.org/10.1038/310641a0, 1984.

Smith, D. C.: A review of the peculiar mineralogy of the "Norwegian coesite-eclogite province" with crystal-chemical, petrological, geochemical and geodynamical notes and an extensive bibliography, in: Eclogites and Eclogite-facies Rocks, edited by: Smith, D. C., 1–206, Elsevier, ISBN: 044443030X, 1988.

Smith, D. C. and Cheeney, R. F.: Orientated needles of quartz in clinopyroxene: evidence for exsolution of SiO_2 from a non-stoichiometric supersilicic "clinopyroxene", in: 26th International Geological Congress, Paris, 02.3.1, 145, Abstracts, 7–17 July 1980, 1980.

Smith, D. C. and Lappin, M. A.: Coesite in the Staumen kyanite-eclogite pod, Norway, Terra Nova, 1, 47–56, https://doi.org/10.1111/j.1365-3121.1989.tb00325.x, 1989.

Smyth, J. R., Bell, D. R., and Rossman, G. R.: Incorporation of hydroxyl in upper-mantle clinopyroxenes, Nature, 351, 732–735, https://doi.org/10.1038/351732a0, 1991.

Spencer, K. J., Hacker, B. R., Kylander-Clark, A. R. C., Andersen, T. B., Cottle, J. M., Stearns, M. A., Poletti, J. E., and Seward, G. G. E.: Campaign-style titanite U–Pb dating by laser-ablation ICP: implications for crustal flow, phase transformations and titanite closure, Chem. Geol., 341, 84–101, https://doi.org/10.1016/j.chemgeo.2012.11.012, 2013.

Spengler, D., Brueckner, H. K., van Roermund, H. L. M., Drury, M. R., and Mason, P. R. D.: Long-lived, cold burial of Baltica to 200 km depth, Earth Planet. Sc. Lett, 281, 27–35, https://doi.org/10.1016/j.epsl.2009.02.001, 2009.

Spengler, D., Alifirova, T. A., and van Roermund, H. L. M.: Subcratonic and tectonic evolution of pyroxenite and eclogite with lamellar inclusions in garnet, Western Gneiss Region, Norway, J. Petrol., 62, egab008, https://doi.org/10.1093/petrology/egab008, 2021.

Terry, M. P. and Heidelbach, F.: Deformation-enhanced metamorphic reactions and the rheology of high-pressure shear zones, Western Gneiss Region, Norway, J. Metamorph. Geol., 24, 3–18, https://doi.org/10.1111/j.1525-1314.2005.00618.x, 2006.

Terry, M. P., Robinson, P., and Krogh Ravna, E. J.: Kyanite eclogite thermobarometry and evidence for thrusting of UHP over HP metamorphic rocks, Nordøyane, Western Gneiss Region, Norway, Am. Mineral., 85, 1637–1650, 2000.

Terry, M. P., Bromiley, G. D., Robinson, P., and Heidelbach, F.: Determination of equilibrium water content and composition of omphacitic pyroxene in an UHP kyanite-eclogite, Western Norway, 6–11 April 2003, Nice, France, Geophys. Res. Abstr., 5, 08698, 2003.

Tucker, R. D., Krogh, T. E., and Råheim, A.: Proterozoic evolution and age-province boundaries in the central part of the Western Gneiss Region, Norway: results of U-Pb dating of accessory minerals from Trondheimsfjord to Geiranger, Special Paper 38, 149–173, Geological Association of Canada, 1990.

Tucker, R. D., Robinson, P., Solli, A., Gee, D. G., Thorsnes, T., Krogh, T. E., Nordgulen, Ø., and Bickford, M. E.: Thrusting and extension in the Scandian hinterland, Norway: new U-Pb ages and tectonostratigraphic evidence, Am. J. Sci., 304, 477–532, https://doi.org/10.2475/ajs.304.6.477, 2004.

van Roermund, H. L. M., Carswell, D. A., Drury, M. R., and Heijboer, T. C.: Microdiamonds in a megacrystic garnet websterite pod from Bardane on the island of Fjørtoft, western Norway: evidence for diamond formation in mantle rocks during deep continental subduction, Geology, 30, 959–962, https://doi.org/10.1130/0091-7613(2002)030<0959:MIAMGW>2.0.CO;2, 2002.

Vrijmoed, J. C., van Roermund, H. L. M., and Davies, G. R.: Evidence for diamond-grade ultra-high pressure metamorphism and fluid interaction in the Svartberget Fe–Ti garnet peridotite–

websterite body, Western Gneiss Region, Norway, Mineral. Petr., 88, 381–405, https://doi.org/10.1007/s00710-006-0160-6, 2006.

Vrijmoed, J. C., Smith, D. C., and van Roermund, H. L. M.: Raman confirmation of microdiamond in the Svartberget Fe-Ti type garnet peridotite, Western Gneiss Region, Western Norway, Terra Nova, 20, 295–301, https://doi.org/10.1111/j.1365-3121.2008.00820.x, 2008.

Vrijmoed, J. C., Austrheim, H., John, T., Hin, R. C., Corfu, F., and Davies, G. R.: Metasomatism in the ultrahigh-pressure Svartberget garnet-peridotite (Western Gneiss Region, Norway): implications for the transport of crust-derived fluids within the mantle, J. Petrol., 54, 1815–1848, https://doi.org/10.1093/petrology/egt032, 2013.

Wain, A.: New evidence for coesite in eclogite and gneisses: defining an ultrahigh-pressure province in the Western Gneiss region of Norway, Geology, 25, 927–930, https://doi.org/10.1130/0091-7613(1997)025<0927:NEFCIE>2.3.CO;2, 1997.

Wain, A., Waters, D., Jephcoat, A., and Olijynk, H.: The high-pressure to ultrahigh-pressure eclogite transition in the Western Gneiss Region, Norway, Eur. J. Mineral., 12, 667–687, https://doi.org/10.1127/0935-1221/2000/0012-0667, 2000.

Walczak, K., Cuthbert, S., Kooijman, E., Majka, J., and Smit, M. A.: U–Pb zircon age dating of diamond-bearing gneiss from Fjørtoft reveals repeated burial of the Baltoscandian margin during the Caledonian Orogeny, Geol. Mag., 156, 1949–1964, https://doi.org/10.1017/S0016756819000268, 2019.

Warren, C. J., Beaumont, C., and Jamieson, R. A.: Deep subduction and rapid exhumation: role of crustal strength and strain weakening in continental subduction and ultrahigh-pressure rock exhumation, Tectonics, 27, TC6002, https://doi.org/10.1029/2008TC002292, 2008.

Yamato, P., Burov, E., Agard, P., Pourhiet, L. L., and Jolivet, L.: HP-UHP exhumation during slow continental subduction: self-consistent thermodynamically and thermomechanically coupled model with application to the Western Alps, Earth Planet. Sc. Lett., 271, 63–74, https://doi.org/10.1016/j.epsl.2008.03.049, 2008.

Young, D. J.: Structure of the (ultra)high-pressure Western Gneiss Region, Norway: imbrication during Caledonian continental margin subduction, GSA Bulletin, 130, 926–940, https://doi.org/10.1130/B31764.1, 2018.

Young, D. J., Hacker, B. R., Andersen, T. B., and Corfu, F.: Prograde amphibolite facies to ultrahigh-pressure transition along Nordfjord, western Norway: implications for exhumation tectonics, Tectonics, 26, TC1007, https://doi.org/10.1029/2004TC001781, 2007.

Zhang, L., Song, S., Liou, J. G., Ai, Y., and Li, X.: Relict coesite exsolution in omphacite from western Tianshan eclogites, China, Am. Mineral., 90, 181–186, https://doi.org/10.2138/am.2005.1587, 2005.